INVESTIGATION OF GULLY EROSION USING ELECTRICAL RESISTIVITY METHOD AND REMOTE SENSING TECHNIQUES IN UGBOWO, UNIBEN, BENIN CITY, EDO STATE, NIGERIA.

BY

OKORAWHE ISRAEL OGHENEVWEDE

B. Sc Physics (UNIBEN)

(PG/PSC2015666)

SUPERVISOR:

PROF. C. O. AIGBOGUN

A THESIS SUBMITTED TO THE SCHOOL OF POSTGRADUATE STUDIES AS PART OF REQUIREMENT FOR THE AWARD OF THE DEGREE OF MASTERS IN APPLIED GEOPHYSICS IN THE DEPARTMENT OF PHYSICS, UNIVERSITY OF BENIN, BENIN CITY, NIGERIA.

OCTOBER, 2023

CERTIFICATION

We hereby certify that this thesis is an original research work carried out independently by OKORAWHE ISRAEL OGHENEVWEDE under the supervision of Prof. C. O. Aigbogun in fulfillment of the requirements for the award of the Degree of Master (M.Sc) in Applied Geophysics, Department of Physics, University of Benin, Benin City-Nigeria.

_____ _____

Prof. C. O. AIGBOGUN DATE

SUPERVISOR

_____ _____

Prof. OSAHON O. D DATE

HEAD OF DEPARTMENT

_____ _____

EXTERNAL EXAMINER DATE

CERTIFICATION OF THESIS/DISSERTATION ON PLAGIARISM

We the undersigned attest and declare that the thesis of Okorawhe Oghenevwede Israel, titled Investigation of Gully Erosion using Electrical Resistivity Method and Remote Sensing Techniques in Ugbowo, Uniben, Benin City, Edo State, successfully passed the anti-plagiarism test and does not violate any copyright regulations.

……	……..……
Prof. C. O. AIGBOGUN	Prof. OSAHON O.D
SUPERVISOR.	HEAD OF DEPARTMENT

DEDICATION

This thesis is dedicated to the Almighty God, my dearest and lovely parents Mr Daniel Okorawhe (late) and Mrs. Yellow Okorawhe, my well-wishers as well as for the benefit of mankind.

ACKNOWLEDGEMENT

I am grateful to God Almighty the creator of all things who has made this project a success.

My sincere gratitude goes to my supervisor, Prof. C. O. Aigbogun whose interest, and guidance has brought this research work to successful end. My appreciation goes to the H.O.D physics Department Prof. Osahon.

I am very grateful to all the physics lecturers who gave me the confidence and academic support to make this work a success.

My deep gratitude goes to my Parents, My spiritual father, Jesus Holiness, St. Dikeji Daniel MiyeriJesu (The Bishop of the Whole World) and family, and my uncle Evang. Peter Avwerosuoghene, Evang. Dr S. O. Olotu, Evang. Mrs. Constance Udemba, Evang and Evang. Mrs. Clement Ekragha, Evang Mrs. Sylvester Oromoni, and the host of others for their support and encouragement throughout the program duration.

TABLE OF CONTENT

CHAPTER THREE

CHAPTER FOUR

CHAPTER FIVE:

LIST OF TABLES

LIST OF FIGURES

ABSTRACT

This study examines gully erosion in Uniben, Ovia North East Local Government Area in Benin City, Edo State, Nigeria, using a combination of remote sensing and electrical resistivity approaches. Using the Wenner-Schlumberger array, fourteen profiles were used for 2D Electrical Resistivity Imaging (ERI), and RES2DINV was used to analyze the results. The Inverted 2D Resistivity structure from the study region is used to portray the data in this model in a color-coded manner.

The section's vertical scale represents the depths, measured in meters, and its horizontal scale represents the lateral distance. A maximum spread of 200 meters was modelled, and all profiles were examined down to a comparable depth of 39.6 meters. The 2-D resistivity structure analysis indicates that alluvium, laterite, and clay are present in the first four layers near the surface (12.6 – 31.9 m), and that this presence increases significantly as one descends (31.9 – 39.6 m) to suggest that sand (alluvium and Laterite) may be the primary cause of the gully in the area. By integrating geoelectric sections derived from the 2D data, the study delineates the lithostratigraphy of the study area, predominantly identifying sand formations down to a depth of approximately 27 meters.

Moreover, the research includes the application of remote sensing techniques to monitor gully development over time and estimate the extent of gully erosion in the area. It encompasses Digital Elevation Models, as illustrated by heat maps, that employ the Normalized Difference Vegetation Index (NDVI) to evaluate the vulnerability of gully erosion in the studied region. The five zones on the NDVI maps are red, yellow, and green, respectively, denoting places that are very vulnerable to gully erosion, areas that are moderately prone, and areas that are less susceptible. NDVI data were calculated for each season during a four-year period, giving a multi-dimensional picture of the environmental changes in the area.

CHAPTER ONE

1.0 INTRODUCTION

1.1 BACKGROUND OF THE STUDY

Soil erosion is the physical removal of materials (soil particles) from one place to another. It is an accelerated process under which soil is bodily displaced and transported away faster than it can be formed.

Soil erosion is caused by the action of water and wind. Rain striking the ground helps to break soil particles loose and then runoff carries away loosened soil. Soil erosion agents can also be anthropogenic factors.

Erosion physically removes materials (soil) in place after weathering (breakdown of rock or mineral materials) has broken them down into smaller pieces that are movable.

Soil erosion starts with rainfall droplets dislodging particles of soil, removing them, and eventually depositing them at a new location different from the original site. The erosion problems of an area are subjected to certain factors which include the geology, land use act, geomorphology, climate, soil texture, nature, and biodiversity of the area.

High torrential rainfall is a significant environmental issue wreaking havoc on southern Ni geria since it fosters a favorable climate for catastrophic soil erosion (Chude et al., 2021). The process by which soil particles are removed, moved, and deposited in a different locati on than their original location where they were produced is known as soil erosion.

Deep cuttings that cut through the entire earth's surface in the area of the incident are the re sult of this.

Due to the striking mark, they leave on the earth's surface, gullies constitute the most obvio us and severe kind of soil erosion (Ofomata, 1981).

It is impossible to overstate the destructive effects of gully erosion on people's lives, bodies, and socioeconomic activities. According to the World Bank Country Report on Nigeria from

2009, gully erosion is one of the top five environmental dangers (Mbaya, 2013). Millions of Naira worth of properties have been destroyed by gully erosion, and many mor e are under danger.

In one instance of gully erosion in the Auchi district of Edo State, almost 10 homes were lo st.

Additionally, it was recently revealed that erosion has destroyed over 450 buildings in the Nigerian state of Edo (NTA News, Sunday, July 6, 2013) (Abdulfatai et al, 2014).

Agriculture, which is recognized as a means of subsistence, is included. Gully's impact puts the nation's food security at danger. Gullies may cause up to $100 million in economic damage annually, with agricultural yield losses of 30 to 90% in some locations, primarily in the southeast of Nigeria (Linus,2020).

It has been determined that gully erosion and landslides are the main causes of the widespr ead breakdown of the transportation and communication networks, the degradation of arabl e land, the contamination of the water supply, the isolation of settlements, and the migratio n of communities in southeast Nigeria (Boniface et al., 2019). Rain and the nature of the soil were found to be the main causes of soil erosion in the Nigerian state of Edo, which includes the Benin city (Omon and Ogheruemusua, 2014). However, attempts to reduce the impending impact of gully erosion by the deployment of tunnels and side drains have not been successful. The study area's slope steepness, weakly developed structure, unconsolidated soil structure, less cohesion, and high permeability, among other factors, contribute to landslides and gully erosion, according to field observations and geotechnical evaluation of gully erosion in Iguosa Benin City Edo State (Aigbadon et al., 2021). Transportation amongst others is a major influence in the socio-economic development and growth of any nation of the world. Out of the many systems of transportation, a larger size of the society carryout the transportation of goods, services and human via road transportation. Roads are constructed from geologic elements, and the engineering characteristics of these materials have an impact on the longevity and functionality of this infrastructure (Meshida, 2006). The technical qualities of the underlying geology and

subgrade materials have also been linked to the frequency of road breakdowns. According to reports, the mineralogical compositions of the underlying geologic materials regulate their engineering properties (Akpan, 2005). Road failures are frequently caused by the poor geotechnical properties of the soils, such as poor bearing capacity, low maximum dry density, high liquid limit, plasticity index, ideal moisture content, California bearing ratio, and excessive compressibility (Ademilua, 2018). In order to effectively handle the threat of gully erosion and landslides, assessment and monitoring of the spatial distribution of gullies and landslides are essential. The degree of soil erosion is quickly and comprehensively analysed via remote sensing. Nosipho (2018) conducted a remote sensing study on gully erosion in the Okhombe Valley, Drakensberg, South Africa, with the goal of assessing the potential utility of the Sentinel - 2 MSI sensor in locating and mapping the geographical distribution of gullies. According to the research findings, the result shows that remote sensing can be used to identify and map gully erosion and landslides. It has been shown that the freely available multispectral Landsat 8 OLI sensor can be effective in mapping the geographical distribution of soil erosion at the regional scale, where substantial fieldwork is constrained by inaccessibility to such places (Seutloali et al., 2017). Despite numerous studies and investigations into the cause(s) of soil erosion in the region, the major reason for the persistent gully erosion that occurs within the Benin city is still unclear and a mystery that needs to be solved. The engineering qualities of the subsurface, which are thought to be a primary driving force in gully erosion and soil erodibility, may now be evaluated indirectly, non-invasively, quickly, and cost-effectively thanks to this scientific work.

1.1.1 Gully Erosion

A gully is a landform created by running water, mass movement, or commonly a combination of both eroding sharply into soil or other relatively erodible material, typically on a hillside or in river floodplains or terraces. Gully erosion occurs when water is channelled across unprotected land and washes away the soil along the drainage lines. Under natural conditions, runoff is moderated by vegetation, which generally holds the soil together, protecting it from excessive runoff and direct rainfall. Gully erosion are more

common during rainy or wet seasons on a huge scale. Water also makes gullies easier by lowering the angle of equilibrium, adding weight, and decreasing friction. Generally speaking, a landslide is caused mainly by gully erosion (Igbokwe et al., 2003). The main causes of soil erosion and gully formation among the numerous factors causing gully formation are erosivity and erodibility. Rainfall, a natural occurrence that is uncontrollable and unavoidable, has an effect on erosion. According to Shi et al. (2012), soil erosion is the process through which top soil particles are detached and transported by wind and/or water. Soil erosion results in the loss of topsoil under the action of water or wind. As a result of soil erosion, sheets, rills, and gullies are formed. When these soil particles are easily carried by flowing water in a thin layer, or sheet, sheet erosion occurs. If this sheet runoff is permitted to concentrate and pick up speed, it cuts rills and gullies while simultaneously separating more soil particles. Gullies turn into deep channels and gorges when slope length and gradient enhance the erosive force of flowing water (Poesen,2011). Gully erosion is a type of soil erosion that involves an open, incised, and unstable channel that is often more than 30 cm deep. It is described as the removal of the top soil along drainage channels by surface water runoff. Gully erosion kinds are the most noticeable types of erosion in Nigeria because of the outstanding imprint they leave on the earth's surface (Ofomata, 1981). It is impossible to overstate the effects of gully erosion. In 1988, a terrible occurrence in Nanka Anambra State, South Eastern Nigeria, forced the evacuation of more than 50 people. According to studies and investigations, this occurrence was caused by a layer of over-consolidated, extremely plastic mudstone with a Plasticity Index (PI) of 67 and a lot of montmorillonite clay (Okagbue, 1992). Gully erosion is however the most prominent feature in the landscape of Edo State and every community in the State has a tale of woe as a result of ever-increasing gullies.

Gully erosion is a highly visible form of soil erosion or an antecedent of the removal of soil by running water that affects soil productivity, restricts land use and can threaten roads, fences and buildings. These develop because of a decrease in the erosion resistance of the

land surface or increase in the erosion forces acting on the land surface. As water channelled across unprotected land, it washes away the soil along the drainage lines.

1.1.2 The Influence of Soil Characteristics

The balance between soil forming processes and soil erosion is depicted by the depth of soil. The soil profile controls the tolerance of a slope to all destabilizing factors. Inclination and orientation of structural surface have the greatest effect on the stability of the slopes (Crozier, 1986). Soil texture determines its ability to absorb and store water, generally this is referred to as liquefaction, a condition when the soil momentarily liquefies and tends to behave as a dense liquid, a condition which is required for landslides to occur. The important textures that control liquefaction are sand and silts or a combination of the two textures (Bryant, 1991; Msilimba, 2002; Msilimba and Holmes, 2005). Gullies are more likely to occur in weaker soils like silt and clay because they share complex (colloids) or numerous planes of weakness (clay-humus complex). High clay-content soils are known to expand when it rains and contract when it's dry (Krhoda, 2013).

1.1.3 Strength of the Soil (Cohesion)

The force that holds together like particles in the structure of soil is known as cohesion. Without any compressive tension, this force is still present. A soil's shear strength is a good indicator of how resistant it is to erosion. It is specifically described as being resistant to deformation caused by tangential (shear) stress. Cohesion between particles and resistance to particles sliding over one another due to friction or interlocking makeup soil shear strength. There are two types of cohesion: genuine cohesion and perceived cohesion. The shear wave velocity of soil layers is a crucial characteristic for assessing soil amplification and liquefaction (Ferhat and Tezegul, 2011).

1.2 GEOLOGY OF NIGERIA

Nigeria lies approximately between latitudes 4°N and 15°N and Longitudes 3°E and 14°E, within the Pan African mobile belt in between the West African and Congo cratons (Fig. 1). The Geology of Nigeria is dominated by three major rock types; the crystalline (igneous and

metamorphic rocks) and sedimentary rocks both occurring approximately in equal proportions. The crystalline igneous and metamorphic rocks constitute the Precambrian - Palaeozoic basement complex which occurs in the eastern region of the country and extends through the north-central to the north-eastern part of Nigeria. The Sedimentary Basins comprises 7 inland basins namely the Niger Delta, the Anambra Basin, the Benue Trough, the Chad Basin, the Sokoto Basin, the Bida-Benue Basin, and the Dahomey Basin, all infill with sediments varying in age from the Cretaceous to recent.

Figure 1.1: Location of Nigeria sandwiched between the West African and the Congo Cratons

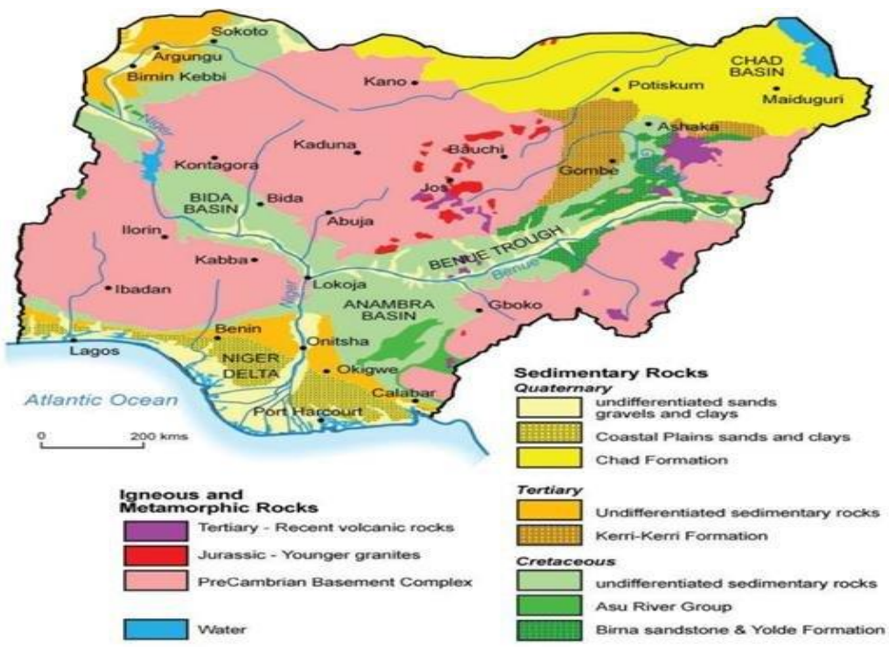

Figure 1.2: Geological Map of Nigeria

1.2.1 REGIONAL GEOLOGY OF NIGER DELTA

The study area, Benin City Edo State falls within the Niger Delta Basin. The basin is an extensive continental margin basin situated in the Gulf of Guinea built out into the Central South Atlantic Ocean at the mouths of the Niger-Benue and Cross River systems during the Eocene. It is an accurate delta that is wave-dominated and tidally influenced sand bodies whose thickness may be influenced by growth faulting (Avbovbo and Ayoola, 1981).

The Niger Delta has an aerial extent of 75,000 km^2 and is located at the southern end of Nigeria bordering the Atlantic Ocean and extends from longitude 3°E - 9°E and latitude 40^0 3'-5°2'N. It is the second-largest delta in the world with a coastline spanning about 450 km terminating at the Imo River entrance (Awosika, 1995). The region spans over 20,000 km^2 and it has been described as the largest wetland in Africa and consists of freshwater swamps, mangrove swamps, beaches, bays, and estuaries. The pro-delta developed in the northern part of the basin during the companion transgression and ended in the Paleocene transgression. The formation of the modern Delta began during the Eocene. The three major depositional environments (marine, mixed and continental) are observable in the Niger Delta and represented by the Benin, Agbada, and Akata Formations.

The term "Benin formation" was first coined in 1907 and later fell into disuse. It was reinstated by Reyment (1965) replacing it with “Coastal plain-sand” which outcrops in Aba, Owerri, and Port-Harcourt areas in eastern Niger Delta province and Warri, Sapele, Eku, Oleh, Ozoro, and Ughelli area of the western Niger Delta. The formation consists predominantly of very thick coastal sands, sandstones, and clay and sandy clay occurring in lenses (Reyment, 1965). Neither of these workers mentioned lignites in the Benin Formation in their formational description, although both mentioned lignites in the Ogwashi-Asaba Formation. However according to (Whiteman, 1982), both disseminated and bedded lignites occur within the Benin Formation. Generally, the Benin Formation can be recognized due to its high sand proportion (70-100%), minor shale intercalations, and absence of brackish water and marine fauna. To date, very little oil has been found and the formation is mainly water-bearing (Whiteman, 1982). However, south of Asaba through Abraka and Sapele to

the coast, it is masked by the younger Holocene deposits of the Sombrero - Warri deltaic Plain Sand with the Mangrove Swamp and Freshwater Swamp wetlands to the West and South-West. The Freshwater Swamps are typically filled by a succession of thinly bedded silts and clays that are interbedded with sands (Allen, 1965; Amajor, 1991; Akpoborie, 2011).

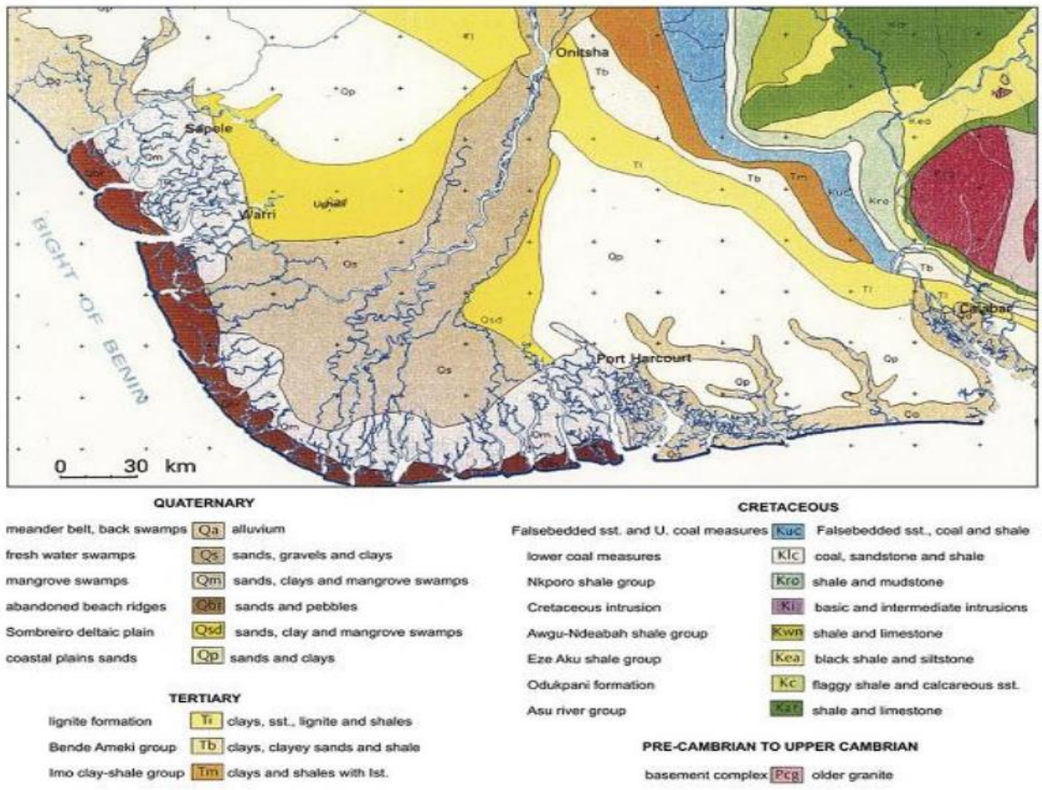

Figure 1.3: Geological Map of Niger Delta (Reijers, 2011).

1.2.2 GEOLOGY OF STUDY AREA

The survey area is located within longitudes 5°36'5.28"E and latitudes 6°20'9.04"N. an elevation of 80.2 Meters (263.14 Feet). The gully site (the University of Benin blocks of flat) is situated in Ovia-North East Local Government Area. The area also occupies the Southern part of Edo State which is a sedimentary terrain and is underlain by sedimentary rocks of Paleocene to recent age. The sedimentary rock contains about 90% of sandstone and shale intercalations (Alile et al., 2011). Edo State is situated in the Southwestern part of Nigeria. It is an important sedimentary basin in Nigeria due to its closeness to the oil fields within the Niger Delta region.

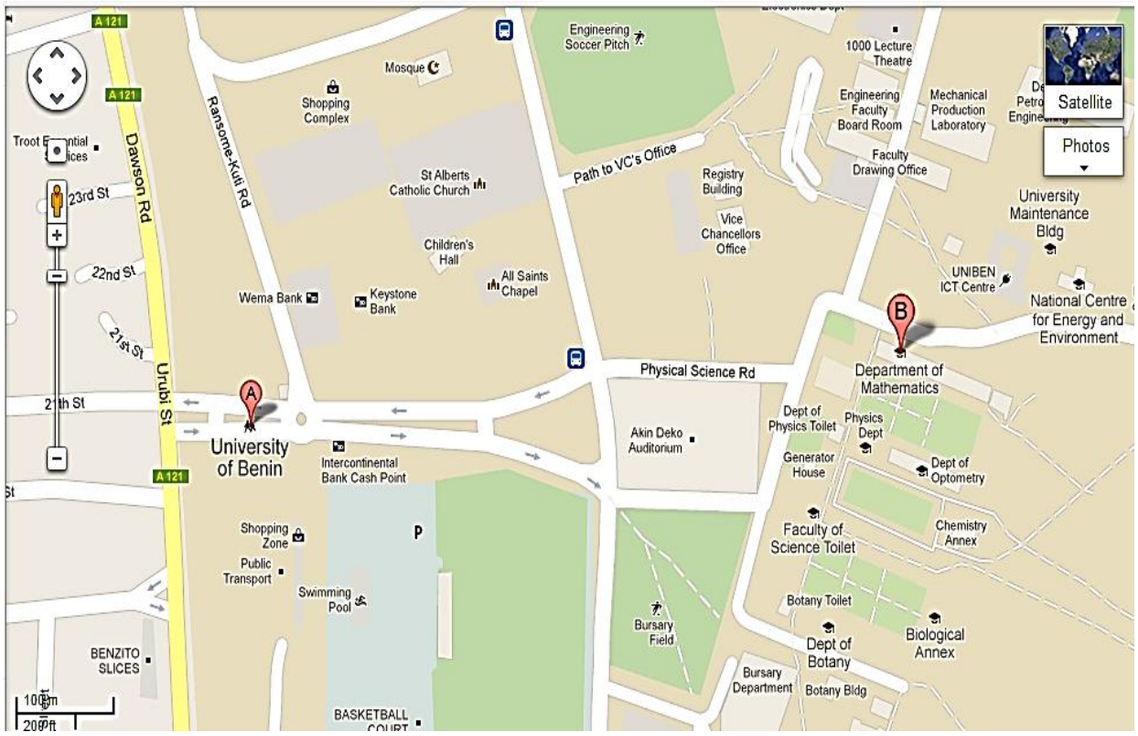

Figure 1.4: A picture of the study area. (Source: Google – Earth)

1.3 Aim and Objectives of the Study

The aim of this study is to carry out the investigation of gully erosion using remote sensing, technique, and electrical resistivity method, a case study of blocks of flat, Uniben, Ovia - North East local govt. area, Benin City, Edo state Nigeria.

The objectives of this study are to:

1. demonstrate the usefulness and enhance appreciation for the techniques of remote sensing, and resistivity techniques in land degradation assessment and proffer possible control measures to tackle the erosion problem.
2. recommend appropriate mitigation of gully erosion in the study area.
3. determine the stiffness of the soil of the study area.

CHAPTER TWO

2.0 LITERATURE REVIEW

2.1 PREVIOUS WORK DONE

Numerous investigations of gully erosion and areas have been conducted over the years. In a study by Wenfu et al. (2008), soil erosion control factors such as soil cape, land cover, terrain, and climatic parameters were integrated with remote sensing and GIS techniques to predict the process of soil erosion in the Yizi region. This method resulted in numerous types of soil erosion hazards in the study area, with numerical values of the Soil Loss Equation (SLE) ranging from low to high. According to study findings, remote sensing, and GIS techniques are effective tools for forecasting the process of soil erosion. Eleraki et al. (2010) used the electrical resistivity method to analyze the appearance of soil water in the core area of Tenth of Ramadan City, Egypt, which poses a significant environmental issue. To determine the relationship between this issue and both lateral and vertical changes of a clay layer that may serve as a geological barrier in the area under consideration, direct current resistivity measurements of 1D and 2D surveys were conducted. In order to determine the distribution of the subsurface layers and identify the anticipated clay barrier, 27 Schlumberger sounding stations were acquired with different spacings based on the local topography and civil constructions. Due to its sensitivity in detecting vertical changes in the subsurface resistivity, a Wenner array electrode design was used. Several interpreted anomalies from the 1D sounding survey were measured along five 2D resistivity profiles. The results of the resistivity inversion demonstrate that within a little distance, the subsurface resistivity varies quickly. However, it was possible to match the resistivity ranges with underlying geological information gathered from shallow boreholes using the models that were produced. The significance of 2D resistivity imaging for measuring the clay barrier layer is demonstrated by this correlation.

In a geographic information system context, Ozsoy et al. (2012) investigated the spatial distribution of yearly soil loss potential in the MKP River Basin using the Revised Universal

Soil Loss Equation (RUSLE) function. The topographic factor was created using an electronic elevation model. The model indicated that the MKP River Basin's overall potential for soil loss due to water erosion might reach 11,296,063 Mg year (-1), with an average soil loss of 11.2 Mg year (-1). Sediment-delivery ratio equations were used and compared with the sediment-monitoring data of the Dolluk stream gauging station on the MKP River in light of RUSLE's limitations in estimating sediment yield for a watershed. The gauge station's estimated sediment yield, which is close to the 127.6 Mg km (-2) year (-1) sediment yield measured at Dolluk sediment gauge station, is 170.2 Mg km (-2) year (-1). This close match demonstrates that the RUSLE function produced in a GIS environment may be used to accurately and reliably assess the prospective soil erosion risk of the MKP River Basin.

Flood Hazard Zones were mapped by Eteh et al. in 2019. In some areas of Yenagoa Metropolis, the use of Geographic Information Systems and Remote Sensing methods. The main causes are cited as increased rainfall, river dredging, a lack of drainage system maintenance, disregard for environmental rules, and other infrastructure. Farms and fishing equipment in coastal towns and communities have been severely impacted as a result of the floodwaters that occurred in Bayelsa State in 2012 and 2018. ArcGIS 10.6 was used to create and analyze the digital elevation model and IDW Contour, the 3D model from ground data, of Yenagoa city using SRTM data. Based on the field study, flood level calculations were made to categorize flood hazard zones for agricultural, construction, and migration purposes.

Seismic refraction tomography (SRT) and electrical resistivity tomography (ERT) were used in a 2D near-surface litho-structural geophysical investigation at the vicinity of two gully-erosion/landslide sites in south-eastern Nigeria by Egwuonwu et al. (2019). P-wave velocity in the modeled SRT data was in the range of 300–2000 ms^{-1}, whereas apparent resistivity in the ERT data was in the range of 1–25,500 m. The ranges cover those of weathered lateritic soil, saturated sandy soil, clay, sandy clay, clayey sand, and sandstones, according to the combined interpretation produced using both methodologies. Clay, sandy clay, and clayey sand were particularly prominent, according to ERT tomograms.

Johnbosco and Ogbonnaya (2021) used an integrated field survey, and hydrological, geotechnical, and geomorphological methodologies to examine the effects of hydro geomorphological variables on gullying processes in erosion-prone geological units in areas of southeast Nigeria. The study area is characterized by numerous shallow groundwater systems and surface water bodies, both of which flow westward from high elevations on the Nanka Formation to low elevations on the Ogwashi and Benin formations, according to the results of the field survey and hydrology. The soils are porous, weak, easily dispersible, and collapsible, according to geotechnical study. According to geomorphological studies, the region is characterized by unlevel bad land topography, steep gully slope gradients, concave slopes, unsatisfactory land-use patterns, and little vegetation cover. The study's findings generally show that the hydro-geomorphology and soil engineering characteristics have a significant impact on the gullying processes in the region. However, because to differences in their hydro-geomorphological properties, regions underlain by the Nanka Formation show higher gullying intensity than regions underlain by the Ogwashi and Benin formations.

Uwaezuoke (2021) used electrical resistivity imaging and multichannel surface wave analysis to study the subsurface of a wetland region in Lagos, Nigeria. The results of the ERI surveys showed that the underlying strata are made up of peat/organic materials with resistivity values between (0.7 and 3) Ω-m, silty clay with values between (5 and 50) Ω-m, and sandy clay sediments with resistivity values between (51 and 105) Ω-m, all of which were mapped at different depths. Additionally, three zones were clearly mapped, as evidenced by the shear wave velocity models derived from MASW observations. The low shear strength strata of peat/organic materials with Vs ranging from (25-70) m/s, silty clay with Vs varying from (70-120) m/s, and sandy clay with Vs ranging from (120-150) m/s are these zones. The combined method has made it easier to establish the boundaries between strata, as well as their thicknesses and uniformity. As a result, it was possible to achieve moderate to very significant correlations between the measured resistivity and velocity and the boreholes that were dug. For each traversal, the regression models were compared rather well. The plotted geological units have an engineering meaning that the location has

weak/incompetent materials that are unsuitable for hosting the foundation of particularly huge structural constructions. Therefore, deep foundations through pilling to the competent layer should be taken into consideration, or soil stabilizing techniques can be used.

Modak *et al.,* (2022) adopted the analytical hierarchy process (AHP) model coupled with geospatial technology in Gully erosion vulnerability modeling, estimation of soil loss and assessment of gully morphology which was carried out on the lateritic terrain of Rupai watershed of eastern plateau fringe of India, where water erosion is a disturbing concern.

According to this study, the watershed contains 31.64% of the moderate risk zone and 49% of the high to very high gully erosion vulnerability zone (GEVZ). This model has been validated using an accuracy evaluation, which yielded a result of 90.91%, and a Kappa co-efficient value of 0.86. The GEVZ was defined using GIS technologies, and the revised universal soil loss equation (RUSLE) model was used to determine the average yearly soil loss. It demonstrates that the watershed's projected average soil loss ranges from < 15 to 431 t ha^{-1} y^{-1}. Around 29% of the study area experiences high to very high (57 to > 147 t ha^{-1} y^{-1}) soil erosion risk, whereas 68% area endures a low level of soil erosion risk (< 15 t ha^{-1} y^{-1}). According to the research on gully morphology, tiny to medium-sized gullies have depths between 1 and 5 meters and are shaped like V and U forms. The study's findings may be used to guide the planning and management of land use and soil erosion control.

The hydrogeological and geotechnical parameters of gully erosion sites in Uturu and its surroundings were evaluated by Nwankwoala et al. in a 2022 study. The area was subjected to severe weathering under tropical and subtropical climatic circumstances, which led to the accumulation of hydrated iron and aluminum oxides, and resulted in sedimentary rocks made of lateritic soils that are covering the area, according to a geological evaluation. The soils at the gully locations had sorting values between 0.42 and 2.3, coefficient of uniformity values between 3.0 and 10, and coefficient of curvature values between the range of 0.2 and 1.3, according to the sieve studies, showing that the soils there are fair to well-sorted. Between 11.0 and 15.0 on the plasticity index.

Maina, M. B. (2022) in his Surveillance of Gully Erosion in Damagum Town and Environs, Fune Local Government Area, Yobe State of Nigeria, used information from primary and secondary sources to map the affected regions and explore the causes of gully erosion. Data from soil analyses, GIS maps, rainfall maps, and other sources were used. The slope, elevation, stream pattern, and flow direction of the affected gully locations across a distance of more than 2000m were also examined using natural elements. This monitoring shows that sand mining is one of the primary anthropogenic and natural sources of the issue of gully erosion.

Adel *et al.,* (2022) carried out a GIS-based simulation of gully erosion development by implementing Python–GIS modules based on the topographic characteristics of the study area, soil properties, and measured runoff. The results reveal that the developed modules allow a successful data simulation and spatial visualization of the obtained results in 2D and 3D as well as a time series analysis of gully evolution.

2.2 REMOTE SENSING

Remote sensing is the study of gathering data about the Earth's surface without coming into close contact with the Earth’s surface. This is actually carried out by sensing and recording the reflected or emitted energy from the earth’s surface and then processing, analyzing, and applying that information. Remote sensing techniques allow taking images of the earth’s surface in various wavelength regions of the electromagnetic spectrum (EMS). The process involves an interaction between incident radiation and the targets of interest.

Remote sensing can be categorized as passive or active, depending on the source of electromagnetic energy. For passive remote sensing, the remote sensing measurements depend upon an external energy source such as sun. Whereas in active remote sensing, the energy source is provided by the remote sensing platform. The majority of remote sensing devices operate in passive mode since they use solar energy as their EMR source. Sensors mounted on airborne or spaceborne platforms capture solar energy reflected by the objects at particular wavelength bands. In remote sensing, wavelength and energy bands that can pass through the atmosphere without experiencing considerable loss due to atmospheric

interactions are typically employed to ensure that there is enough signal intensity received at the sensor. Any object which is at a temperature above 0^{o} K (Kelvin) emits some radiation, which is approximately proportional to the fourth power of the temperature of the object. As a result of its 300^{o}K average temperature, the Earth also produces some radiation. The brightness of the Earth can also be measured by passive sensors, albeit their use is less common due to their low energy content.

2.3 SENSOR SYSTEMS

2.3.1 Camera/Sensor Platforms

Platform is the stage/structure where a camera/sensor is mounted in order to acquire information about a target under investigation. As described by Lillesand and Kiefer (2000), a platform is a vehicle, from which a sensor can be operated. There are three broad categories of remote sensing platforms: ground based, airborne, and satellite platforms.

2.3.2 Ground-based Platforms

A wide variety of ground-based platforms are used in remote sensing. Some of the more common ones are hand held devices, tripods, towers and cranes. Instruments that are ground-based are often used to measure the quantity and quality of light coming from the sun or for close range characterization of objects. For example, to study properties of a single plant or a small patch of grass, it would make sense to use a ground-based instrument.

Laboratory instruments are used almost exclusively for research, sensor calibration, and quality control. Much of what is learned from laboratory work is used to understand how remote sensing can be better utilized to identify different materials. This contributes to the development of new sensors that improve on existing technologies.

Field instruments are also largely used for research purposes. This type of remote sensing instrument is often hand-held or mounted on a tripod or other similar support

2.3.3 Airborne Platforms

Airborne platforms were the sole non-ground-based platforms for early remote sensing work. The first aerial images were acquired with a camera carried aloft by a balloon in 1859. Balloons are rarely used today because they are not very stable and the course of flight is not always predictable, although small balloons carrying expendable probes are still used for some meteorological research.

At present, airplanes are the most common airborne platform. Nearly the whole spectrum of civilian and military aircraft is used for remote sensing applications. When altitude and stability requirements for a sensor are not too demanding, simple, low-cost aircraft can be used as platforms. However, as requirements for greater instrument stability or higher altitudes become necessary, more sophisticated aircraft must be used.

Another class of aircraft that has been in use for many years is remote control aircraft or drones. Remotely controlled aircraft are often used for conditions when it may be too hazardous to fly. They have been used extensively by the military.

2.3.4 Satellite Platforms

The most stable platform aloft is a satellite, which is space-borne. The first remote-sensing satellite was launched in 1960 for meteorological purposes. Now, over a hundred remote sensing satellites have been launched and more are being launched every year. The Space Shuttle is a unique spacecraft that functions as a remote-sensing satellite and can be reused for a number of missions.

Satellites can be classified by their orbital geometry and timing. Three orbits commonly used for remote sensing satellites are geostationary, equatorial, and Sun-synchronous. A geostationary satellite has a period of rotation equal to that of Earth (24 hours) so the satellite always stays over the same location on Earth. Communications and weather satellites often use geostationary orbits with many of them located over the equator. In an equatorial orbit, a satellite circles Earth at a low inclination (the angle between the orbital plane and the

equatorial plane). The Space Shuttle uses an equatorial orbit with an inclination of 57 degrees.

Sun-synchronous satellites have orbits with high inclination angles, passing nearly over the poles. Orbits are timed so that the satellite always passes over the equator at the same local sun time. In this way, the satellites maintain the same relative position with the sun for all of their orbits. Many remote sensing satellites are Sun-synchronous which ensures repeatable sun illumination conditions during specific seasons. Because a Sun-synchronous orbit does not pass directly over the poles, it is not always possible to acquire data for the extreme polar regions. The frequency at which a satellite sensor can acquire data on the entire Earth depends on sensor and orbital characteristics. For most remote sensing satellites, the total coverage frequency ranges from twice a day to once every 16 days.

Most remote sensing satellites have been designed to transmit data to ground-receiving stations located throughout the world. To receive data directly from a satellite, the receiving station must have a line of sight to the satellite. If there are not sufficient designated receiving stations around the world, any given satellite may not readily get a direct view of a station, leading to potential problems of data discontinuity. To work around this problem, data can be temporarily stored onboard the satellite and then later downloaded upon acquiring contact with the receiving station. Another alternative is to relay data through TDRSS (Tracking and Data Relay Satellite System), a network of geosynchronous (geostationary) communications satellites deployed to relay data from satellites to ground stations.

2.4 ELECTROMAGNETIC SPECTRUM

For remote sensing to occur, there must be an energy source to illuminate the target (unless the sensed energy is being emitted by the target) which is usually in the form of electromagnetic radiation. All electromagnetic radiation has fundamental properties and behaves in predictable ways according to the basics of wave theory. Electromagnetic radiation consists of an electrical field (E) which varies in magnitude in a direction perpendicular to the direction in which the radiation is traveling, and a magnetic field (M)

oriented at right angles to the electrical field. Both of these fields travel at the speed of light (c). Two characteristics of electromagnetic radiation are particularly important to understand remote sensing. These are the wavelength and frequency. Electromagnetic radiation (EMR) is an electromagnetic wave that travels through space at the speed of light C (3 x 10^8m/s). Theoretical models of random media including the anisotropic effects, random distribution discrete scatters, and rough surface effects, have been studied for remote sensing with electromagnetic waves. The relationship between the parameters that characterize an EM wave is given by:

$$\mathbf{c = f\lambda} \qquad \mathbf{2.1}$$

Where f is the frequency and λ is the wavelength

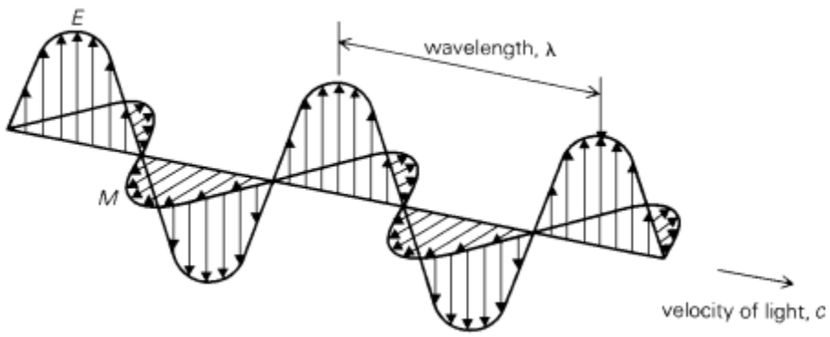

Figure 2.1: EM Wave with Electric Field E and Magnetic Field M, both perpendicular to the direction of propagation.

Electromagnetic energy radiates in accordance with the basic wave theory which describes EM energy as traveling in a harmonic sinusoidal fashion at the speed of light. Notwithstanding, many characteristics of EM energy are easily described by wave theory, another theory known as particle theory offers insight into how electromagnetic energy interacts with matter. It suggests that EMR is composed of many discrete units called photons/quanta. The energy of a photon is given by

$$\mathbf{E = \frac{hc}{\lambda} = hf} \qquad \mathbf{2.2}$$

Where E is the energy of quantum,

h = Planck's constant with a numerical value of 6.63×10^{-34} m^2 kg/s

2.5 ENERGY INTERACTIONS WITH SURFACE FEATURES OF THE EARTH

Depending on the wavelength and the properties of the surface (such as plants, water bodies, or bare soil), energy incident on the earth's surface is absorbed, transmitted, or reflected. The way that electromagnetic radiation interacts with surface features depends on both the qualities of the incident radiation and those of the features. Following interaction with the surface features, energy that is reflected or reemitted from the features is captured by the sensors and analysed to pinpoint the target features, calculate the object's distance from the sensor, and/or determine its properties.

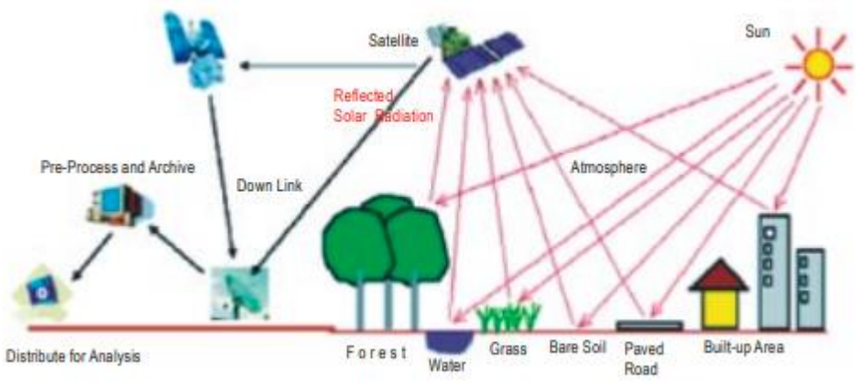

Figure 2.2: Remote Sensing Process

2.5.1 Energy Interactions

The incident electromagnetic energy may interact with the earth surface features in three possible ways: Reflection, Absorption and Transmission. These three interactions are Reflection Absorption Earth Transmission incident radiation Reflection occurs when radiation is redirected after hitting the target. According to the law of reflection, the angle of incidence is equal to the angle of reflection the EM energy which is absorbed by the earth’s surface is available for emission and as thermal radiation at longer wavelengths. Transmission occurs when radiation is allowed to pass through the target. Depending upon the characteristics of the medium, during the transmission velocity and wavelength of the radiation changes, whereas the frequency remains same. The transmitted energy may further get scattered and/or absorbed in the medium. These three processes are not mutually exclusive. Energy incident on a surface may be partially reflected, absorbed or transmitted. Which process takes place on a surface depends on the wavelength of the radiation, angle at

which the radiation intersects the surface and composition and physical properties of the surface. The relationship between reflection, absorption and transmission can be expressed through the principle of conservation of energy. Let E_I denote the incident energy, E_R denotes the reflected energy, E_A denotes the absorbed energy and ET denotes the transmitted energy. Then the principle of conservation of energy (as a function of wavelength λ) can be expressed as

$$\mathbf{E_I(\lambda) = E_R(\lambda) + E_A(\lambda) + E_T(\lambda)} \qquad \mathbf{2.3}$$

Since most remote sensing systems use reflected energy, the energy balance relationship can be better expressed in the form:

$$\mathbf{E_R(\lambda) = E_I(\lambda) - E_A(\lambda) - E_T(\lambda)} \qquad \mathbf{2.4}$$

The reflected energy is equal to the total energy incident on any given feature reduced by the energy absorbed or transmitted by that feature.

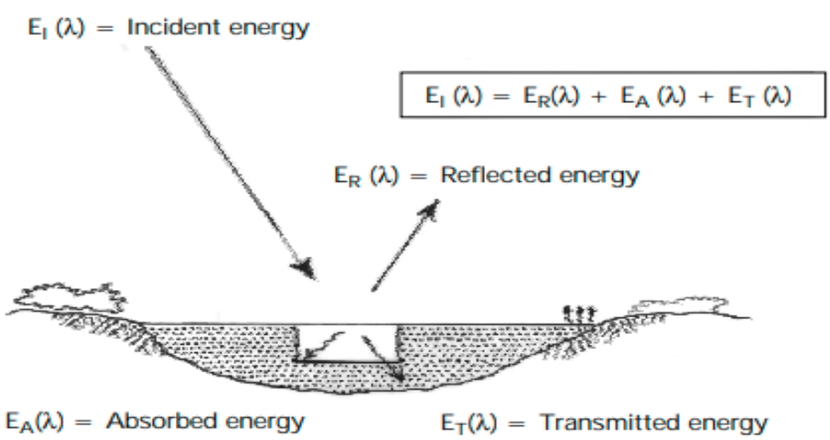

Figure 2.3: Interaction of Energy with the earth's surface. (Lillesand and Kiefer, 1994)

2.6 GEOGRAPHIC INFORMATION SYSTEM (GIS)

Geographic Information System (GIS) helps in determining the changes in land use and land cover in different areas. Accordingly, GIS is able to detect any changes that may occur in land use or cover at a given time. Sudden changes in land use and land cover occur due to natural causes or manmade activities such as cutting down trees, landslides, gullies, etc. Geographic Information Systems (GIS) are tools that are very efficient in the storage management, and display of spatial data generated for the management of the environment,

water resources and soil. Mapping flooding risk areas helps in the evaluation of the potential level in the neighbouring area and also, the damage caused by floods can be estimated and shown using digital maps with the aid of GIS.

GIS has been defined in a variety of ways by many scientists depending on the purpose for which it is applied. According to Burrough (1986), GIS as a set of tools for collecting, storing, retrieving a twill, transforming and displaying spatial data from the real world for a particular set of purpose. Chorley (1987) referred to GIS as a system for capturing, sorting, checking, integrating, manipulating, analyzing, and displaying data that are spatially referenced.

2.6.1 Components of GIS

An enormous amount of geographically-related data must be handled (managed) and analyzed by a geographic information system (GIS). GIS components essentially consist of hardware, software, and, most significantly, an operational database. The diagram below shows the five parts of a GIS.

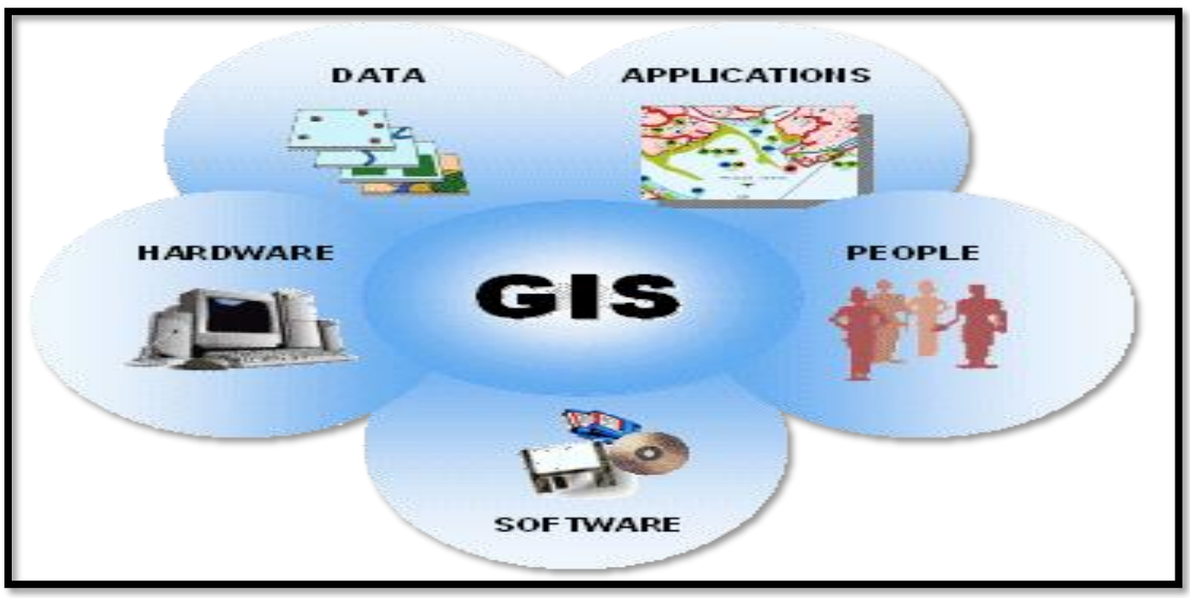

Figure 2.4: Components of GIS (Heywood, 1998).

2.6.2 Software

An enormous amount of geographically-related data must be handled (managed) and analyzed by a geographic information system (GIS). GIS components essentially consist of hardware, software, and, most significantly, an operational database. The diagram below shows the five parts of a GIS.

2.6.3 Hardware

For data processing and storage, a GIS depends on a computer. The GIS operation would determine the system's required size. Smaller GIS projects only need a single computer to run, however, larger GIS projects would require many computers for multiple users. Hardware includes displays, scanners, printers, processors, and other devices.

2.6.4 Data

Geographic or spatial data and attribute-based or non-spatial data are the two types of data used in GIS. Data with a specific geographic location in the form of a set of coordinates are referred to as spatial data. Data with attributes are descriptive sets that include numerous details pertinent to a specific location, such as height, names, depth, width, etc. Additionally, they can be connected to a specific location using an identifier, such as an address, postcode, etc. The utilization of spatially referenced data in GIS is an essential component of providing new information that is just as useful as the original information provided for problem-solving and decision-making. GIS has the ability to gather data from many sources and integrate it in various ways in order to address specific spatial issues.

Spatial challenges are those that necessitate making decisions over a specific area or place (Adeniran et al., 2010). Therefore, solving a spatial problem requires solving a spatial problem. GIS has "modelling" capabilities that support decision-making by providing what-if answers in practical situations.

2.6.5 People

These individuals are those most adept at applying GIS, particularly in specific applications of GIS. They are the persons who use the system and would apply and manipulate GIS to

resolve geographic and spatial tasks. Operators of geographic information systems are responsible for all aspects of the system's daily operation, and they frequently carry out tasks that make it easier for system operators to accomplish their duties well.

2.6.6 Applications

GIS systems are created and developed to support an organization's data management and decision-support procedures. Any organization's operations are founded on a set of procedures and principles that are specific to that organization. The success of any GIS project is greatly influenced by the application and methodology employed. The numerous GIS applications span a wide range of fields, including socioeconomic government, defense organizations, business and trade, utilities, and environmental management. GIS is typically used to model solutions to spatial problems in decision-making. Therefore, it can be seen that GIS has a variety of application fields. Therefore, it can be seen that GIS has a variety of application fields. GIS application areas are:

- Mapping
- Transportation Planning
- Agricultural Value Chain
- Urban Planning
- Disaster Risk and Management
- Natural Resources Management
- Public Health

Table 2.1: Application Areas of GIS

Activity	Application
Commerce and Business	Market share analysis, insurance, fleet management, direct marketing, target marketing, retail site to location
Defense Agencies	Target site identification, tactical support planning, mobile command modeling, intelligence data integration
Environmental Management	Landfill site selection and mineral mapping, potential pollution monitoring, natural hazard assessment,resource management, environmental impact assessment
Socio-economic/Government	Health, Local Government, transport planning, service planning, urban management.
Utilities	Network management, service provision, telecommunications, emergency repairs

2.7 CONCEPT OF ELECTRICAL RESISTIVITY METHOD

In environmental research, civil engineering, and hydrological prospecting, electrical resistivity tomography (ERT) is a commonly used geophysical imaging technique. 2D geoelectrical resistivity tomography has been effectively applied by several researchers to engineering studies for site investigation and characterization (Ahzegbobor et al.2010; Ayolabi et al. 2013). Previous studies have validated the use of the 2D ERT method for the identification of bedrock structures, cavities or sinkholes, and slope stability investigation (Marescot et al. 2008; Perrone et al 2014).

The outcome provided a precise picture of the subsurface structure. Panda KP, Sharma S, and Jha MK (2018) used an electrical approach to map lithological changes in a river basin in West Bengal, India. electrical resistivity analysis. Other array configurations and Wenner

alpha experiments were carried out. The outcome displays a distinct underlying structure. It has been demonstrated that Wenner has good resistivity.

Regional applications of electrical resistivity tomography (ERT) in complicated geological environments have been made (Dahlin and Loke, 1998; Griffiths and Barker, 1993; Amidu and Olayinka, 2006; Aizebeokhai et al., 2010). More trustworthy images of the subsurface top can now be obtained thanks to the recent availability of automated data-collecting equipment and effective, user-friendly inversion software.

Electrical resistivity is one of the most sensitive geophysical methods for monitoring changes in electrical properties in the subsurface (Aizebeokhai et al, 2010).

Geophysical approaches can map subsurface lithologic units and hidden geological structures (Omosuyi et al., 2007). As a result, geophysics is important for mapping subsurface geologic sequences and geological structures.

Electrical Resistivity Tomography survey has been widely used in order to solve engineering, archaeological, environmental, and geological problems in the last decades (Loke, 2003). The electrical resistivity surveying method has undergone dramatic changes over the last two decades. A major improvement since the early 1990s is the development of two-dimensional (2-D) imaging surveys that provide a more realistic model of the subsurface even in complex geological areas.

2.7.1 RESISTIVITY SURVEY TECHNIQUES

There are three types of techniques employed in the resistivity method. These are;

1. Horizontal profile (HP) Technique
2. Vertical Electrical Sounding (VES) Technique
3. Combine horizontal profile and vertical electrical sounding.

2.7.2 Horizontal Profiling Technique

In this technique, profiling is typically conducted with fixed electrode spacing. By moving this electrode array from location to location along a profile, a series of apparent resistivity measurements are made. The lateral variation in ground apparent resistivity is measured using an electrode array with constant spacing in horizontal profiling techniques. Following each measurement, the entire array with constant spacing is shifted. The method measures lateral changes in ground resistivity in relation to a set depth. A plot of apparent electrical resistivity against distance or maps (contour) are used to display the data gathered while in profiling mode.

2.7.3 Vertical Electrical Sounding (VES) Technique

In this method, the vertical variation in ground apparent resistivity values is assessed to a constant electrode array center. According to Alile et al (2008), the survey is conducted by gradually widening the electrode spacing about the array's center. According to Alile, and Amadasun (2007), the electrical resistivity data obtained in the sounding mode are displayed as a bi-logarithmic plot of electrical resistivity vs the distance from the current electrodes to the center of the array. The Schlumberger Array is an example. VES employs collinear arrays designed to output a 1-D vertical apparent resistivity versus depth model of the subsurface at a specific observation point. In this method, a series of potential differences are acquired at successively greater electrode spacing while maintaining a fixed central reference point. The induced current passes through progressively deeper layers at greater electrode spacing. The potential difference measurements are directly proportional to the changes in the deeper subsurface. Apparent resistivity values calculated from measured potential differences can be interpreted in terms of overburden thickness, water table, and the depths and thicknesses of subsurface strata.

2.7.4 Combine horizontal profile and vertical electrical sounding

Despite being in a vertical sense or slice, measurement is two-dimensional. For the sake of accuracy, the data may be inverted. (Aigbogun, et al 2017) Data gathered in the profiling-sounding mode are provided in pseudo section style with the apparent electrical resistivity shown as a function of position and electrode separation.

2.7.5 WENNER-SCHLUMBERGER CONFIGURATION

Wenner-Schlumberger configuration is a configuration with a constant system of spacing rules with a note of factor "n" as this configuration is the comparison of the distance between C_1-P_1 (or C_2-P_2) electrodes with spaces between P_1-P_2 (Loke and Dahlin 2002). If the distance between the potential electrodes (P_1 and P_2) is "a" then the distance between the current electrode (C_1 and C_2) is $2na + a$. The resistivity determination process uses 4 electrodes placed in a straight line. This configuration is a combination of the Wenner configuration and Schlumberger configuration. In the measurement by the spacing factor (n) = 1, the Wenner-Schlumberger configuration is similar to the measurement in the Wenner configuration (distance between electrode = a), but on the measurement with n = 2 and so on, the Wenner-Schlumberger configuration is the same as the Schlumberger configuration. The current electrode and the potential electrode are greater than the distance between the potential electrode.

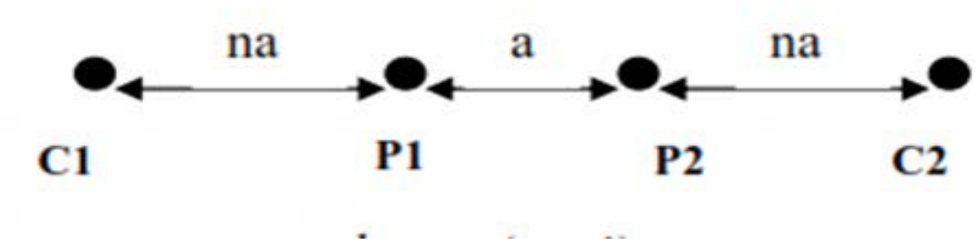

Figure 2.5: Configuration form Wenner-Schlumberger and geometry factor k.

CHAPTER THREE

3.0 MATERIALS AND METHOD

3.1 FIELD SURVEY METHOD - MEASUREMENT PROCEDURE

The use of 2-D electrical imaging tomography surveys to map regions with fairly complex geology is one of the new developments in recent years (Griffiths and Barker 1993). To conduct such surveys, 20 or more electrodes attached to a multi-core wire are typically used. Automatic selection of the appropriate four electrodes for each measurement is done using a laptop CPU and an electrical switching device (Figure 3.1). Field methods and tools for 2-D resistivity studies are currently pretty well developed.

The standard configuration for a 2-D survey is seen in Figure 3.1 by a series of electrodes strung along a straight line and connected to a multi-core wire. Typically, electrodes are spaced apart consistently. A laptop computer is connected to an electrical switching unit, which is where the multi-core cable is hooked.

A text file that can be read by computer software on a laptop is typically used to record the measurement sequence, the type of array to use, and other survey parameters (such as the current to use). You must consult the instructions for your system as different resistivity meters utilize various file formats for the control file. The computer program then automatically chooses the proper electrodes for each measurement after reading the control file. The majority of the fieldwork in a typical survey is spent setting up the wire and electrodes. Waiting for the resistivity meter to finish the set of measurements takes up the majority of survey time! The coverage of the measurements must also be in 2-D for a clear 2-D image of the subsurface to be obtained. 21 electrodes were employed in a wenner-schlumberger electrode array. "a" is the distance between neighboring electrodes.

Making every measurement that can be made using the wenner-schlumberger array with a "1a" electrode spacing is the initial stage. The first measurement is performed using electrodes 1, 2, 3, and 4. Where electrode 1 serves as the first current electrode C_1, electrode 2 as the first potential electrode P_1, electrode 3 as the second potential electrode P2, and

electrode 4 as the second current electrode C_2. During the second measurement, C_1, P_1, P_2, and C_2 are represented by electrode numbers 2, 3, 4, and 5, respectively.

This is carried out again along the electrodes until the final measurement with "1a" spacing is made using electrodes 17, 18, 19, and 20. There are 17 (21 - 4) possible measurements for the Wenner-Schlumberger array with "1a" spacing for a system with 21 electrodes. The subsequent sequence of measurements with "2a" electrode spacing is taken after the series of measurements with "1a" spacing is finished. The initial measurement is conducted using first electrodes 1, 3, and 5. The electrodes are selected using "2a" as the distance between neighboring electrodes. Electrodes 2, 4, 6, and 8 are utilized for the second measurement. Along the line, this procedure is repeated until the final measurement with spacing "2a" is made using electrodes 14, 16, 18, and 20. It should be noted that there are 14 possible measurements with "2a" spacing for a system with 20 electrodes (20 – 2x3)

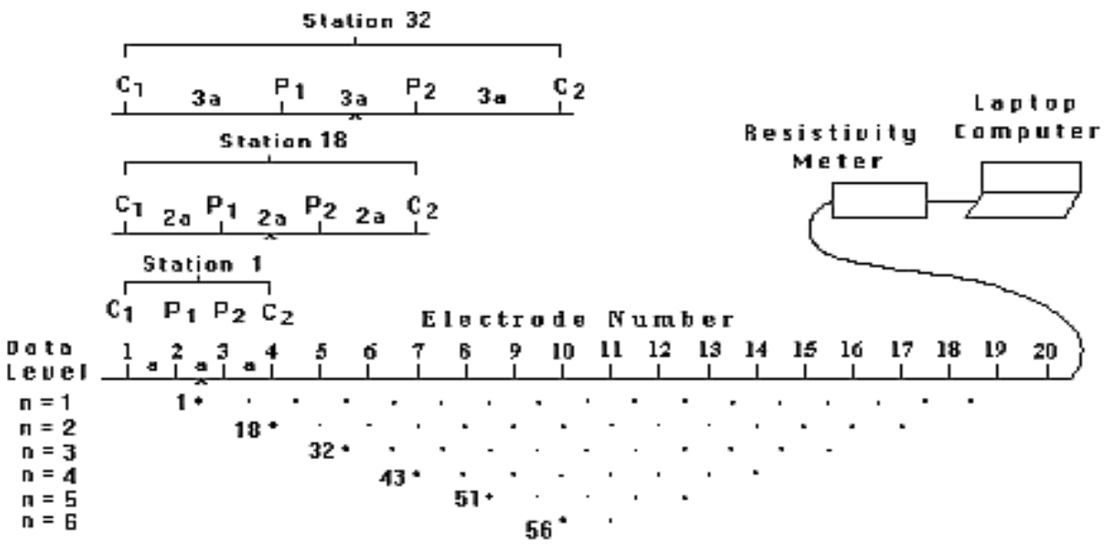

Figure 3.1: The arrangement of electrodes for a 2-D electrical survey and the sequence of measurements used to build up a pseudosection.

For measurements with "3a", "4a", "5a", and "6a" spacing, the same procedure is performed. The measurements in a field survey should be performed methodically to ensure that, to the greatest extent possible, all the potential measurements are made to obtain the best findings. This will have an impact on how well the interpretation model created by inverting the apparent resistivity readings performs (Dahlin and Loke, 1998).

The number of measurements reduces as electrode spacing widens. The type of array chosen will determine how many measurements can be made for each electrode spacing for a specific number of electrodes along the survey line. A total of 14 traverse was taken.

3.2 ELECTRICAL RESISTIVITY METHOD

Electric current (I) is passed into the ground through current electrodes (A and B) during field measurements using the electrical resistivity method, and the potential difference (V) between potential electrodes (M and N) is measured. The quotient of the values of V and I and the geometrical elements of the electrode arrangement used to create the medium's resistivity (Aigbogun *et al.*, 2017).

Imagine a cylindrical conductor with a cross-sectional area of A and a length L. (Figure 3.2). Assumed current (I) is passed via the cylinder's resistance (R), which is given as;

$$R \alpha \frac{L}{A} \tag{3.1}$$

$$R = \rho \frac{L}{A} \tag{3.2}$$

Where the resistivity measured in ohm-meters (m) serves as the proportionality constant. Ohm's law establishes a connection between resistance and the current potential difference (V).

$$\Delta V \ \alpha \ I \tag{3.3}$$

$$\Delta V = IR \tag{3.4}$$

$$\frac{\Delta V}{I} = R \tag{3.5}$$

Combining equation (3.1) and (3.4).

$$\rho \frac{L}{A} = \frac{\Delta V}{I}$$

$$\rho = \frac{A \Delta V}{IL} \tag{3.6}$$

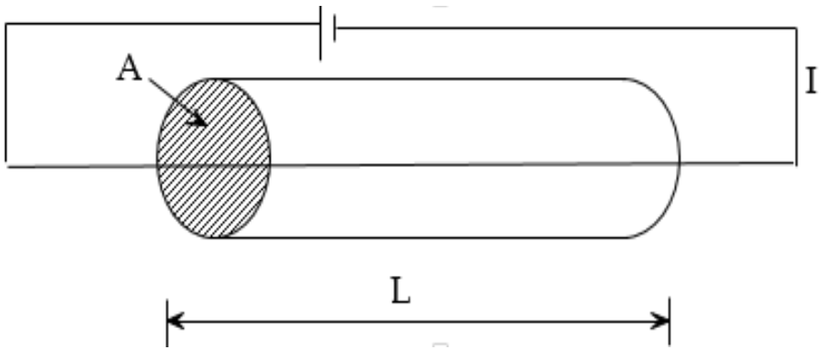

Figure 3.2: A cylindrical conductor. (L = Length, A = Cross sectional area and I= Current)

Any homogeneous or isotropic medium's resistivity can be calculated using equation (3.5), as long as the geometry is straightforward. Cylinders, cubes, and parallel pipe are some examples. It is necessary to define the resistivity at each location of a semi-infinite media. A and L in equation (3.5) cannot be determined in this situation. Hence, by forcing parameters A and 1/L to become infinitesimal,

$$\rho = \frac{\lim_{L \to 0} \frac{\Delta V}{L}}{\lim_{A \to 0} \frac{I}{A}} = \frac{E}{J} \qquad (3.7)$$

Where, $J = \sigma E$ or $J = \frac{E}{\rho}$ (3.8)

Consider the case when the current source is located in the middle of a sphere with a radius of r. (Figure 3.2). As the area of the sphere, A, and the total current, I, are inversely proportional, the current density J will be perpendicular to this surface, constant, and such that

$$J = \frac{I}{A} \qquad (3.9)$$

Therefore; $$J = \frac{I}{4\pi r^2} \qquad (3.10)$$

Substituting for J in equation (3.6)

Then; $$E = \frac{\rho I}{4\pi r^2} \qquad (2.11)$$

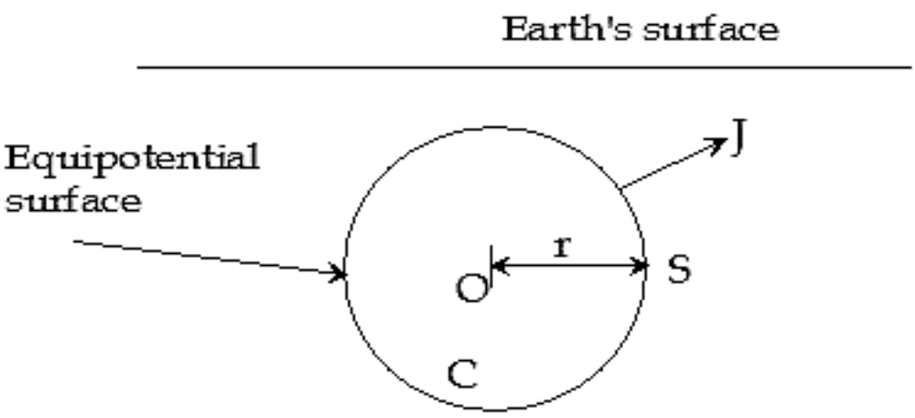

Figure 3.3: Buried current source within a Homogenous Earth.

(C = Current electrode, I = Current density, S = Surface of sphere, r = Radius of sphere)

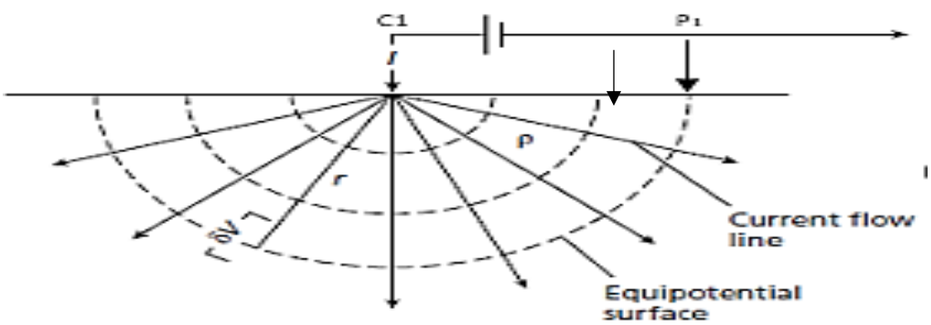

Figure 3.4: Current (C_1) and Potential (P_1) Electrodes on a Homogeneous Half-space (Earth's surface).

Where,

$$J = \frac{E}{\rho}$$

But electric field is equivalent to scalar potential, that is

$$E = -\Delta V \qquad (3.12)$$

$$E = \frac{-\delta v}{\delta r} \qquad (3.13)$$

Equating (2.9) and (2.12) $$\frac{\delta v}{\delta r} = \frac{-\rho I}{4\pi r^2} \qquad (3.14)$$

Integrating equation (2.14) with respect to r, we have;

$$V = \int \frac{-I\rho}{4\pi r^2}\delta r = \frac{-I\rho}{4\pi r}\int \frac{1}{r^2}\delta r \qquad (3.15)$$

$$V = \frac{I\rho}{4\pi r} \qquad (3.16)$$

This is the potential in a spherical structure's center (Figure 3.1). As a result, the potential of a point source is inversely proportional to the medium's resistivity and the current I, and it decreases with increasing distance from the source (r).

The shape of the earth's surface closely resembles a hemisphere in reality (Figure 3.2). The region through which the total current flows will therefore be twice as large in a point source on the surface of the Earth than in an infinite medium. Such that,

$$V = \frac{I\rho}{4\pi r} \times 2 \qquad (3.17)$$

Therefore,

$$V = \frac{I\rho}{2\pi r} \qquad (3.18)$$

Equation (3.16) is the potential at P_1 due to the current supplied at point C_1 on the earth's surface.

3.3 GENERALIZED APPARENT RESISTIVITY EQUATION

In most cases four electrodes are used in resistivity (Figure 3.3)

The potential at P_1 due to current at C_1 is given as

$$V_{11} = \frac{I\rho}{2\pi r_1} \qquad (3.19)$$

The potential at P_1 due to current at $C_{2.}$ is given as

$$V_{12} = \frac{I\rho}{2\pi r_2} \qquad (3.20)$$

The potential contribution V_{11} and V_{12} from the current source C_1 and the sink C_2 are added to create the potential (V_{11}, V_{12}) at an interval electrode P_1.

$$V_{11,12} = V_{11} + V_{12} \qquad (3.21)$$

$$V_{11,12} = \frac{I\rho}{2\pi r_1} + \frac{-I\rho}{2\pi r_2}$$

$$V_{11,12} = \frac{I\rho}{2\pi r_1}\left[\frac{1}{r_1} - \frac{1}{r_2}\right] \quad (3.22)$$

Potential at P_2 due to C_1

$$V_{21} = \frac{I\rho}{2\pi r_3} \quad (3.23)$$

Potential at P_2 due to C_2

$$V_{22} = \frac{-I\rho}{2\pi r_4} \quad (3.24)$$

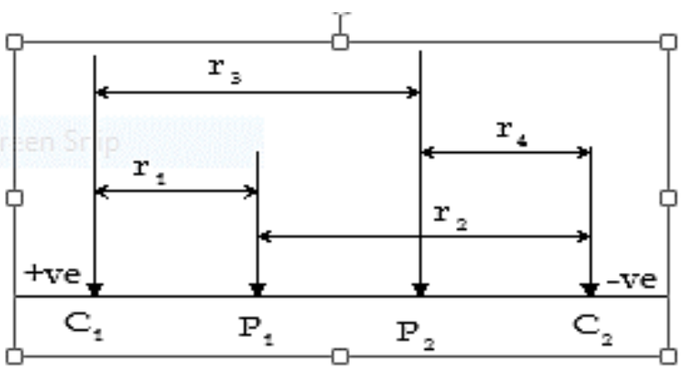

Figure 3.5: Four Electrodes Configuration

The potential at an internal electrode P_2 is equally the sum of the potential contributions V_{21} and V_{22} from the current source and sink C_1 and C_2 respectively,

That is,

$$V_{21}, V_{22} = V_{21} + V_{22} \quad (3.25)$$

$$V_{21}, V_{22} = \frac{I\rho}{2\pi r_3} + \frac{-I\rho}{2\pi r_4}$$

$$V_{21}, V_{22} = \frac{I\rho}{2\pi}\left[\frac{1}{r_3} + \frac{-1}{r_4}\right] \quad (3.26)$$

Since absolute potentials are difficult to monitor, hence the potential difference (ΔV) between electrodes C_1 and C_2 is measured (Keary and Brokes, 1991).

$$\Delta V = V_{11}, V_{12} - {}_{21}, V_{22} \tag{3.27}$$

$$\rho = \frac{2\pi\Delta V}{I}\left[\frac{1}{r_1} - \frac{1}{r_2} - \frac{1}{r_3} + \frac{1}{r_4}\right]^{-1} \tag{3.28}$$

Since, R = ΔV/I

$$\therefore \rho = 2\pi R\left[\frac{1}{r_1} - \frac{1}{r_2} - \frac{1}{r_3} + \frac{1}{r_4}\right]^{-1} \tag{3.29}$$

This is the generalized resistivity equation for any electrode array system. Equation (3.29) could also be written as ρ = GR

Where G is the geometric factor of the array.

$$G = \left[\frac{2\pi}{\frac{1}{r_1} - \frac{1}{r_2} - \frac{1}{r_3} - \frac{1}{r_4}}\right] \tag{3.30}$$

3.4 SURVEY METHOD (WENNER-SCHLUMBERGER)

This experiment used electrical resistivity tomography (ERT), which offers 2-D data on subsurface resistivity, depth, and thickness. ERT is frequently used to identify subsurface geologic units and detect pollutants. In the research area, two (2) profiles were made utilizing the Wenner Schlumberger array arrangement. The travel distance (spread) varied from 0 to 200 meters. One current electrode (C 1), two potential electrodes (P 1 and P 2), and a second current electrode (C 2) make up the Wenner Schlumberger array. With Wenner, the current and potential electrodes are gradually moved down the traverse line while remaining fixed at a regular fixed distance from one another (beginning at a = 5m).

The geometric factor (K) for the Wenner array equals 2πa. Measurements commenced at one end of the traverse line with electrode spacing a=5 m at electrode positions 1, 2, 3, and 4. Next, each electrode (and) was shifted a distance of 5 m, the active electrode positions being 2, 3, 4, and 5. The procedure was continued to the end of the traverse line (as shown in Figure 4). At each measurement, the resistivity meter displayed the field resistance value and the

corresponding root mean square (rms) error of the reading. The apparent resistivity of the subsurface can be computed using the formula = 2πaR for Wenner configuration where a is the electrode spacing distance and R is the field resistance value.

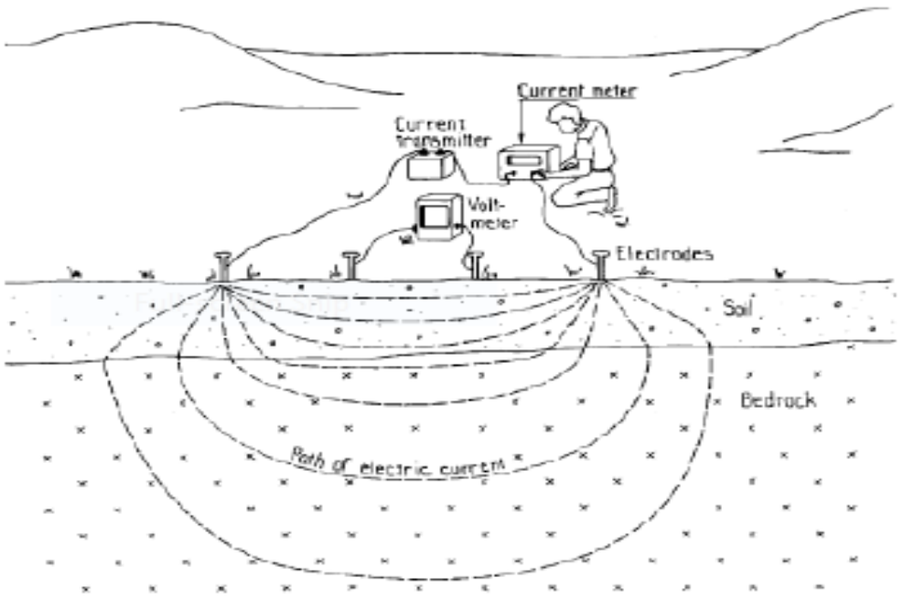

Figure 3.6: Principle of resistivity measurement (modified from Robinson and Coruh, 1988).

Accurate readings were acquired by putting a current of 2A into the earth, which is received on the instrument as resistance values, with the resistivity meter and researchers in position. Using the RES2DINV software, the 2D data sets were inverted to produce a 2D model.

3.5 MATERIALS

The data was acquired using the following equipment and accessories;

- PASI Tetrameter 16GL model
- Thirty-one metal electrodes
- Four hammers for driving the electrodes in the ground
- Crocodile clips
- Two measuring tapes for measuring the distances for the different electrode spacing
- Global Positioning System 72 (GPS) for finding the position and elevation of the survey point
- Power supply- 12V 60Ah battery

- Umbrella
- Four reels of 2 blue and 2 red coloured electric cable
- Base map and
- Data sheet for recording the field data

1. Metal Electrodes: Metal stakes are almost always used as electrodes to inject electricity into the ground; in dry ground, they may need to be driven more than 50 cm into the ground and watered to improve contact. The use of salt water and several stakes is possible where contact is very poor. A hole may need to be blasted through extremely resistant caliche or laterite surface layers in extreme circumstances. Angle-iron lengths with points have bigger contact surfaces and are just marginally less durable. Metal stakes are almost always used as electrodes to inject electricity into the ground; in dry ground, they may need to be driven more than 50 cm into the ground and watered to improve contact. The use of salt water and several stakes is possible where contact is very poor. A hole may need to be blasted through extremely resistant caliche or laterite surface layers in extreme circumstances. Angle-iron lengths with points have bigger contact surfaces and are just marginally less durable.

2. Measuring Tape*:* The length of this plastic strip or roll is marked off in feet, meters, centimetres, and inches. It is used to gauge how far the potential and current electrodes stretch out. When the spread is completely used up but there are still distances to cover, measured distances on the ground can be marked, making the tape available to complete the task.

3. Cables: The cables used are traditionally single core, multi-strand copper wires insulated by plastic or rubber coatings. Thickness is usually dictated by the need for mechanical strength rather than low resistance, since contact resistances are nearly always very much higher than cable resistance. Steel reinforcement may be needed for long cables. The cables incorporate heavy gauge conductors with excellent insulation to ensure good survey results. The cables are expandable for deeper penetration by connecting them in series with a cable joint. The cables are wound on reels.

4. **Pasi Earth Resistivity Meter***:* It is compact, lightweight, and made of durable, weatherproof cast aluminum. It is a system that averages signals. This technique involves taking automatic readings at regular intervals and constantly averaging the findings.

5. **Battery:** This is used to power the Pasi Earth resistivity meter. It is also the source of the current which is sent into the earth, from which the potential difference across the potential electrodes is measured.

6. **Hammer:** The hammer was used to drive the current electrode into the earth subsurface.

7. **Global Positioning System (GPS)***:* A GPS signal is used to calculate precise location, altitude, and velocity, as well as the current time of a geographical area. This is needed for accurate analysis of the position of subsurface anomalies.

3.6 GIS AND REMOTE SENSING DATA PROCESSING

GIS is use in so many areas of earth science like in soil science, geophysics geology, geography and other area of environment science for predication and monitory. The Geographic Information System (GIS) and Statistical approaches are regarded as ground-breaking methods in the assessment of water quality (Arulbalaji, *et al*., 2019). Therefore, GIS is a working tool for data management, data analysis, spatial data display, and non-spatial data analysis.

Google Earth explorer and ArcGIS 10.7.1 were the software used in the collection and processing of the data for this research work.

The data were collected using handheld Global Positioning System (GPS) in degree, minute, second and google earth explorer and transferred to Geographical Information System environment in Data base in Arc GIS 10.7.1 using Arc map tools and add various layers such as road and settlements to generate sample location map, Geologic map.

Spatial analyst extension tools in Arc GIS 10.7.1 using hydrological tools to generate/calculate the fill, flow direction flow accumulation and Euclidean distance to produce Digital Elevation Model.

3.6.1 WORKING ON THE DEM FILE

After the DEM file was generated, it was then converted to TIN (Triangular Irregular Networks) and Raster. Using the raster calculator, the following were calculated; the fill, the flow direction, flow accumulation, and Euclidean distance. Also, the NDVI (Normalized Difference Vegetation Index) was calculated, using the relation:

$$NDVI = float(\frac{Band\ 5 - Band\ 4}{Band\ 5 + Band\ 4}) \qquad (3.31)$$

The procedures are stated below:

Convert the DEM file to TIN on the ArcGIS software → click search and search for contour (spatial analyst tool) → input the clipped file on the input raster box (note the contour interval should be 80) and allow to process → search for create TIN → click on create TIN (3D Analyst) → click on input features and input the contour file created→ click on output features and input Nigeria_LGAs and save the file → coordinate system → projected coordinate system → search for WGS1984 UTM ZONE 32N → click ok → ok.

Next, convert the TIN created to Raster by searching for TIN to RASTER → click on the TIN to Raster (3D Analyst) → save file as Raster file.

Next slope was calculated from the spatial Analyst Tool → search for Reclassify and click on Reclassify (Spatial Analyst) Tool and click ok.

Next fill was calculated by clicking on the ArcTool box → Spatial Analyst Tools → hydrology → fill → reclassify_slope → ok.

Next flow direction was calculated by clicking on the ArcTool box → Spatial Analyst Tools → hydrology → flow direction → ok. The next is flow accumulation using the same process above.

Next the Euclidean distance was calculated using the Raster calculator (which is located in the ArcTool box → Spatial Analyst Tools → Map Algebra → Raster calculator) by inputting "flow Acc_Flow" > = 500 and click ok.

Next stream link was created (under hydrology) → input flow Acc _ flow → flow Dir _ fill. In the same process, the stream order and stream to feature was created.

Next the Euclidean distance was resolved by clicking on Spatial Analyst Tools (under Geoprocessing) → Distance → Euclidean distance → stream to feature → ok. Then the Euclidean distance was reclassified by going to reclassify → input Eucli Dist _ Stre 1.

Next road was created by clicking on add data icon on the ArcGIS software → Nigeria shape files → Roads → edit → Euclidean distance → Environment → processing extent → input the clipped file → ok → ok. After the Roads have been created it was the reclassified by inputting Euclidean distance as input then click ok.

Next the Normalized Difference Vegetation Index was calculated by clicking the Nigeria LGA (study area) → edit → start editing. After this has been created it was then clipped and reclassified.

CHAPTER FOUR

4.0 RESULTS AND DISCUSSION

4.1 RESULTS AND INTERPRETATION

The 2D Electrical Resistivity models are shown in Figures 4.1 to 4.14. In this model, the results are presented in a colour-coded presentation from Figures 4.1 to 4.14 consisting of the Inverted 2D Resistivity structure obtained from the study area. The horizontal scale on the section is the lateral distance while the vertical scale is the depths, which are both in meters. A maximum spread of 200 m was modelled with the corresponding depth of 39.6 m investigated on all the profiles as show from Figures 4.1 to 4.14.

2D ELECTRICAL RESISTIVITY IMAGES OBTAINED FROM FIELD RECORD FOR LOCATION ONE (BLOCKS OF FLAT GULLY SITE UNIBEN)

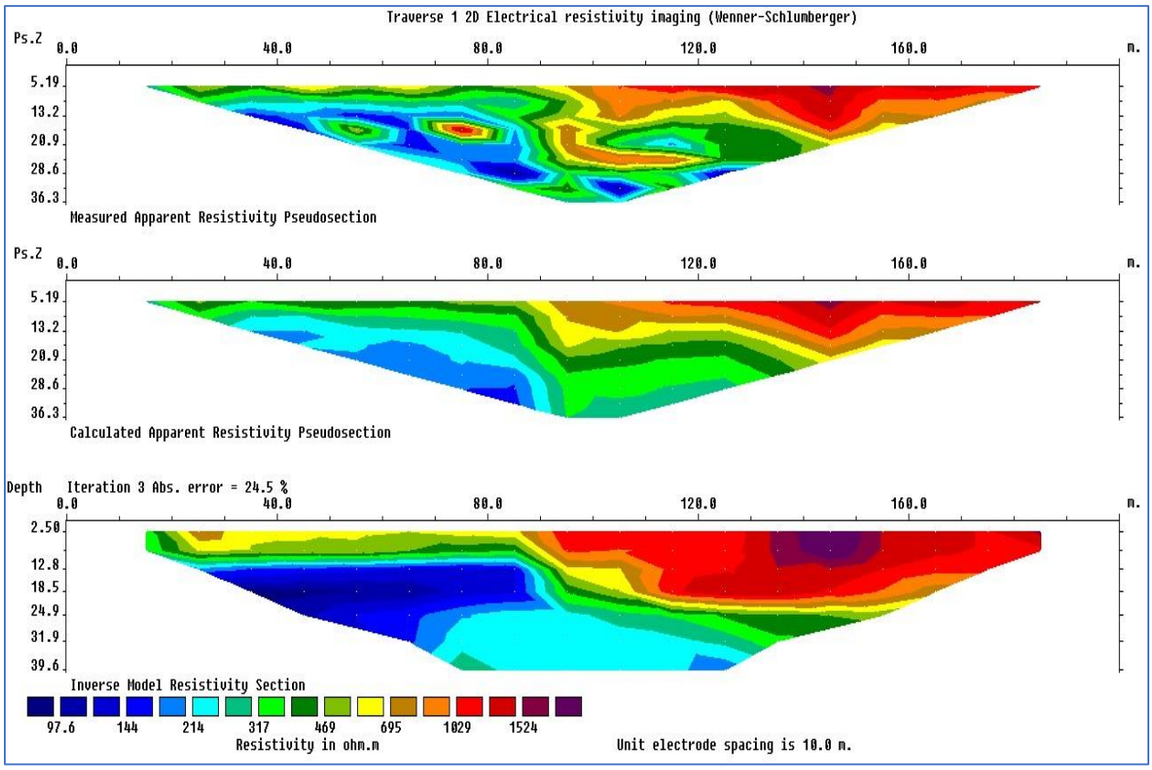

Figure 4.1a:2-D Electrical Resistivity Structure along Traverse One.

4.1.1 2-D Resistivity Section along Traverse One

The 2D resistivity section along traverse 1 is presented in Figure 4.1a. Lateral distance of 200 m was covered and a depth of 39.6 m is imaged. Resistivity values vary from 97.6 – 1524 Ωm across the traverse (Figure 4.1a). Three resistivity structures are delineated which are indications of clayey sand, lateritic sand and sand. The resistivity of the clayey sand varies from 97.6 – 144 Ωm having lateral distance of 25 – 85 m with depth of 12.6 – 31.9 m

along the traverse. The lateritic sand occurs at lateral distance of 85 – 185 m having resistivity values ranging from 1029 – 1524 Ωm with corresponding depth of 2.5 – 18.5 m (as a near-surface structure). The sand occurs at depth of 2.5 – 12.8 m and 24.9 – 39.6 m having resistivity values ranging from 214 - 695 Ωm with lateral distances 15 – 80 m and 70 – 120 m respetively. The high near-surface resistivity values of the resistivity structures are indicative of dry and unconsolidated geologic earth materials which are highly erodible (Karim *et al*., 2019). The near-surface along this traverse is thus suspected to be prone to deep seated erosion due deep depth distributions of the high resistivity values (Figure 4.1a).

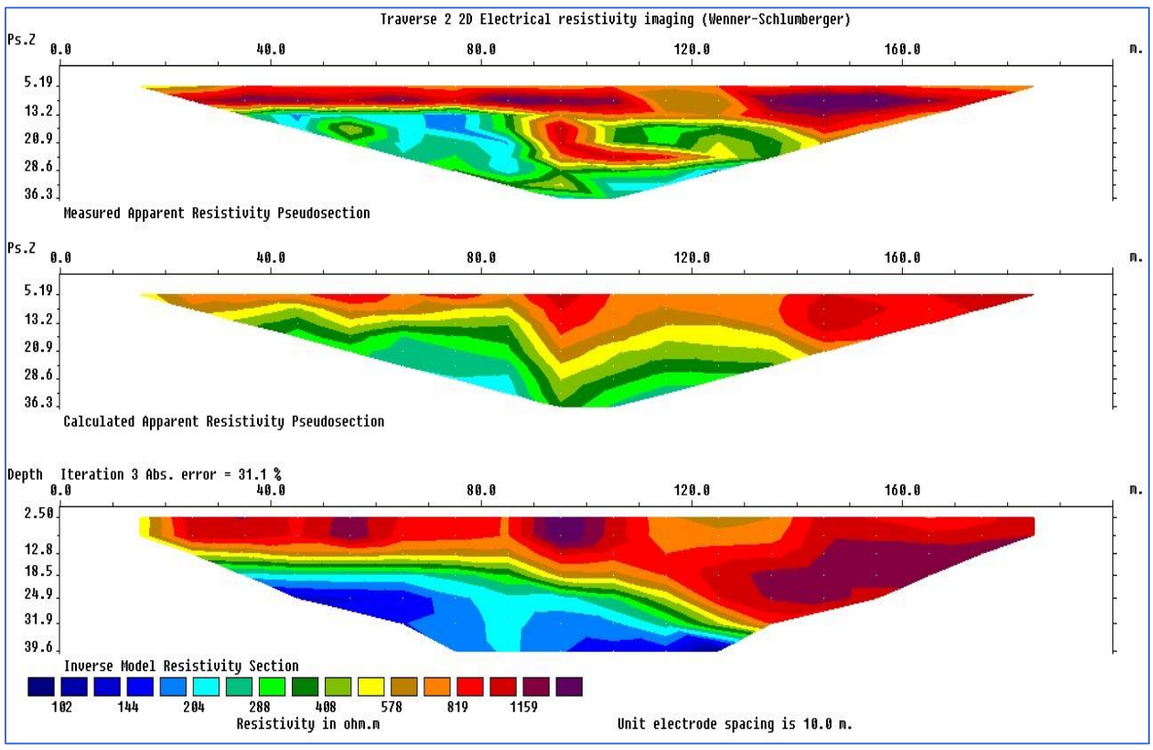

Figure 4.2a:2-D Electrical Resistivity Structure along Traverse Two.

At a horizontal span of 200 m and a depth of 39.6 m, Traverse 2 depicts the 2D resistivity image obtained for Profile Two. The resistivity values for the profile range from 102 m to 1159 m.

The primary rock types in this profile are primarily sedimentary rocks, including shale and sandstone. From a depth of 2.5m to about 31.9 across the profile line of about 10m to 200m rocks with high resistivity from about 578-1159Ωm was suspected indicating the presence of sandstone, shale etc. From a depth of 24.9m down to the last depth, clay, alluvium, laterite where suspected havinig a resistivity values ranging from 102 Ωm-408 Ωm.

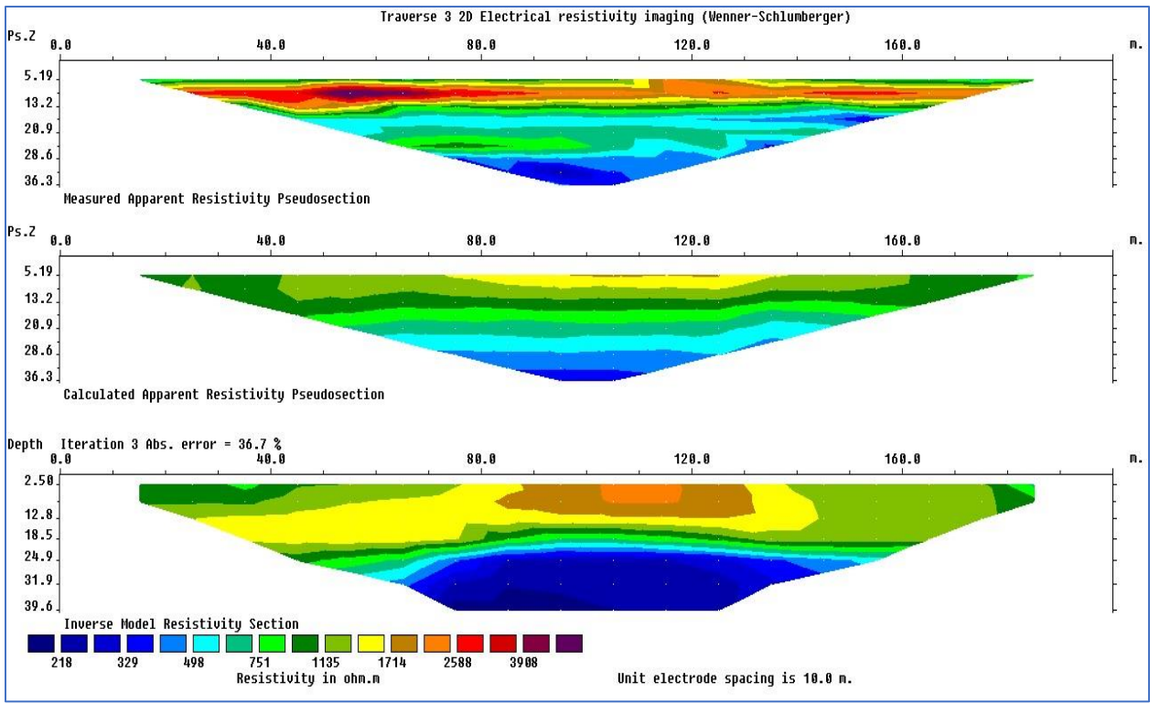

Figure 4.3: 2-D Electrical Resistivity Structure Along Traverse Three.

Figure 4.3 represents the 2D resistivity image obtained for profile three with a horizontal distance of 200 m and a depth of 39.6 m, with resistivity values ranging from 218 Ωm – 3908 Ωm across the profile.

At the top layer I infer from the moderate resistivity that is characterize by Alluvial soil and laterite soil. having a lateral continuity to a distance of about 190m having a resistivity range between 500m – 800 Ωm and laterite soil. Patches of sandstone deposit and shale having a resistivity value of 1135 Ωm-3988 Ωm between a distance of 15m to140m across a depth of 12.0m to 24.9m was inferred. Clay deposit alongside other rocks was inferred in the last layer from a depth of 31.9m -39.6m.

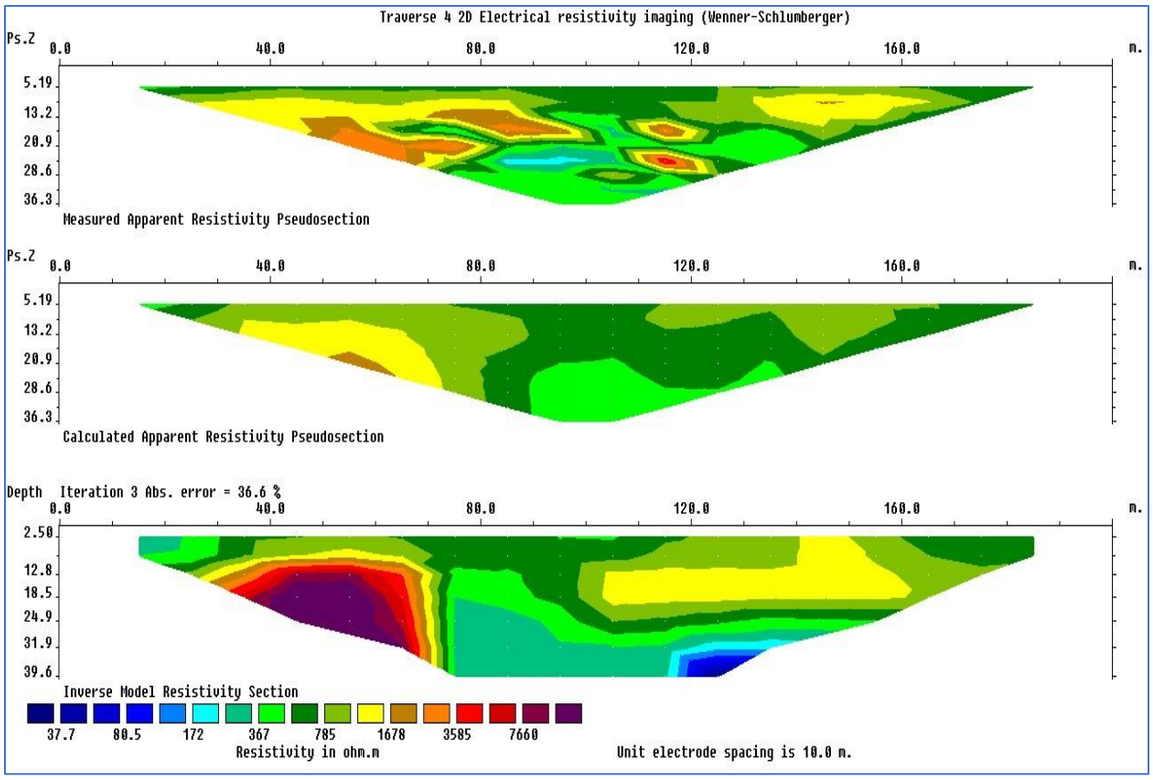

Figure 4.4: 2-D Electrical Resistivity Structure along Traverse four.

Figure 4.4 represents the 2D resistivity image obtained for profile four with a horizontal distance of 200m and a depth of 39.6m, with resistivity values ranging from 37.7 Ωm – 7660 Ωm across the profile.

At the top layer I infer from the moderate resistivity that it is characterize by Alluvial soil, Laterite soil and at a distance of 20 m – 180 m and a depth of 2.50m – 39.6m. Traces of shale and sandstone with resistivity values of 1678 Ωm-7660 Ωm where inferred between a distance 0f 30m -70m, 100m- 150m at a depth of 12.8m-31.6m. Small quantity of clay deposit was suspected at a depth of 31.9m-39.6m across a distance of 120m 140m having a resistivity values of 37.7 Ωm-100 Ωm

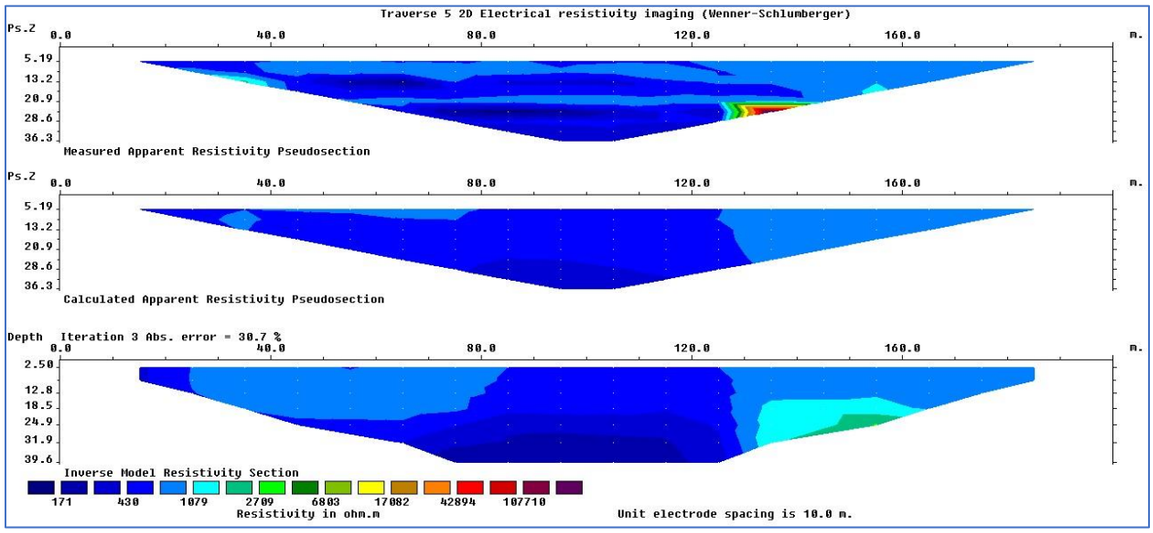

Figure 4.5: 2-D Electrical Resistivity Structure along Traverse five.

Figure 4.5 represents the 2D resistivity image obtained for profile five with a horizontal distance of 200m and a depth of 39.6m, with resistivity values ranging from 171Ωm – 107710 Ωm across the profile.

At the top layer between a distance of 10m to 80m and 130m to 180m between a depth of 2.50m to 24.9m shale having a resistivity of 1079 Ωm -2000 Ωm and sandstone with resistivity value of 2709 Ωm-6803 Ωm was inferred. Clay deposit and clayey sand where inferred at a depth of 24.9m-39.6m and at a distance of 80m – 120m with resistivity value of 1 Ωm to 100 Ωm was suspected.

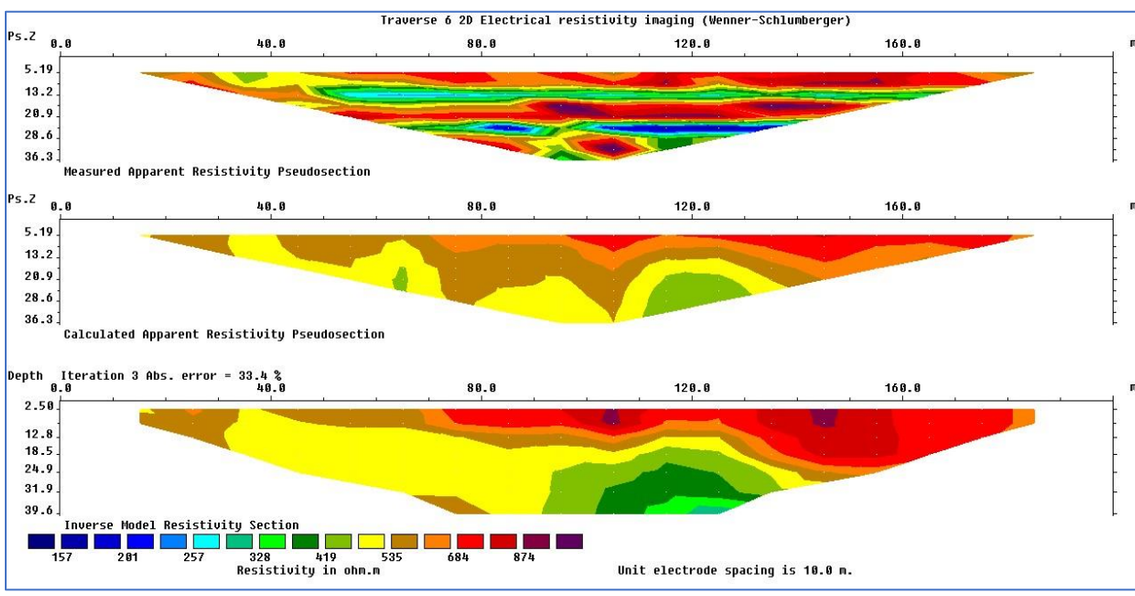

Figure 4.6: 2-D Electrical Resistivity Structure along Traverse Six.

Figure 4.6 represents the 2D resistivity image obtained for profile six with a horizontal distance of 200m and a depth of 39.9m, with resistivity values ranging from 157Ωm – 874 Ωm across the profile.

At the top layer of a depth of 2.50m down to a depth of 31.9m unconsolidated sandstone and shale having a resistivity value of 535 Ωm-874 Ωm across a distance of 10m-180m was inferred. Patches of alluvial and laterite soil were suspected at distance between 90m-140m at a distance of 18.5m down to the last depth.

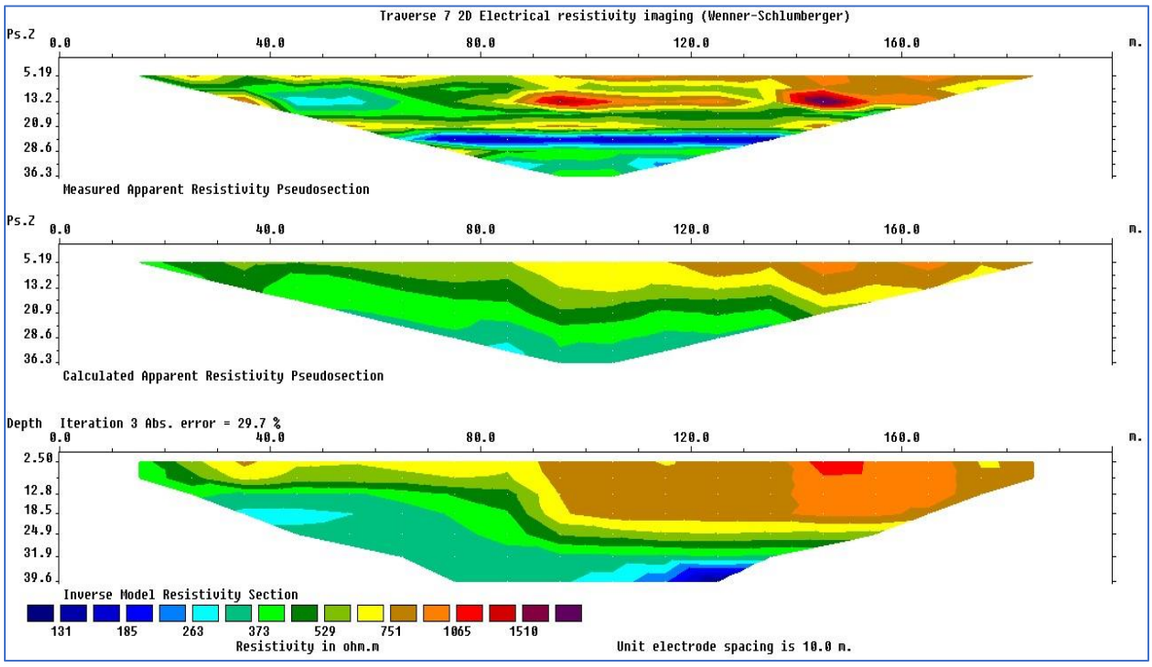

Figure 4.7: 2-D Electrical Resistivity Structure Along Traverse Seven.

Figure 4.7 represents the 2D resistivity image obtained for profile seven with a horizontal distance of 200m and a depth of 39.6m, with resistivity values ranging from 131 Ωm – 1510 Ωm across the profile.

At the top layer, I infer from the moderate resistivity value that is characterize by Alluvial soil, Laterite soil having a resistivity range between 373 Ωm – 751 Ωm, from a depth of 2.50m to 18.5m along a distance of 40m -110m and 160m – 260m sandstone was suspected. Shale and other rocks were inferred at different distances and depths.

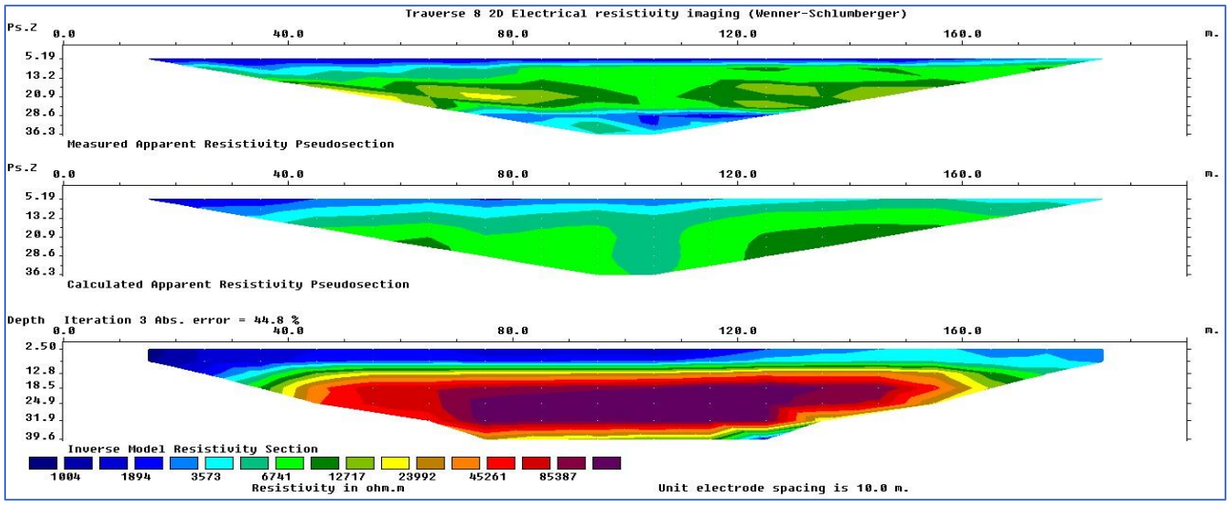

Figure 4.8: 2-D Electrical Resistivity Structure Along Traverse Eight.

Figure 4.8 represents the 2D resistivity image obtained for profile eight with a horizontal distance of 200m and a depth of 39.6m, with high resistivity value to a very high resistivity value across the profile of 1004Ωm – 85387Ωm

At the top layer a high resistivity ranging from 1004 Ωm-3573 Ωm at a depth of 2.50m to 18.5m sandstone and shale was inferred. At a depth of 18.5m to 31.9m a cave like structure suspected to be filled with consolidated sandstone, shale and other rocks including a minute quantity of clay was inferred.

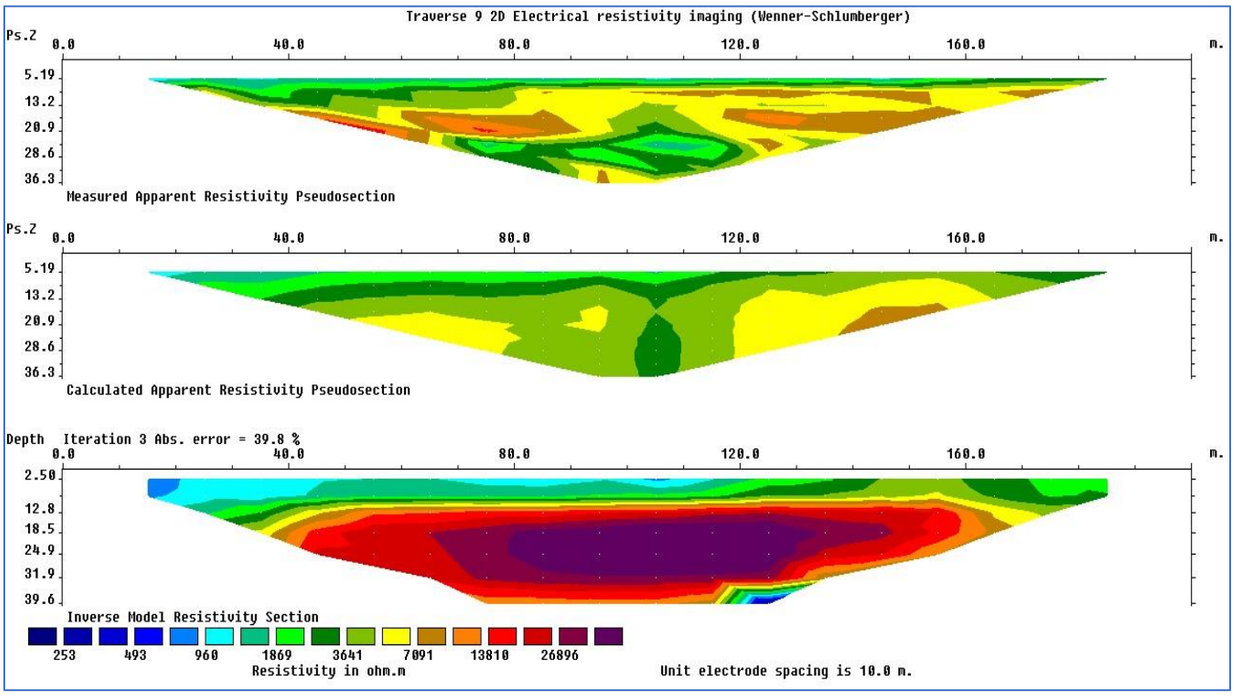

Figure 4.9: 2-D Electrical Resistivity Structure Along Traverse Nine.

Figure 4.9 represents the 2D resistivity image obtained for profile nine with a horizontal distance of 200m and a depth of 39.6m, with a moderate resistivity value to a very high resistivity value across the profile of 253Ωm – 26896Ωm

At the top layer a moderate to high resistivity values ranging from 253 Ωm-7091 Ωm at a depth of 2.50m to 18.5m alluvial, laterite, sandstone and shale was inferred. At a depth of 18.5m to 39.6m a cave like structure suspected to be filled with consolidated sandstone, shale and other rocks having a resistivity value of 13810 Ωm – 26896 Ωm including a minute quantity of clay was inferred.

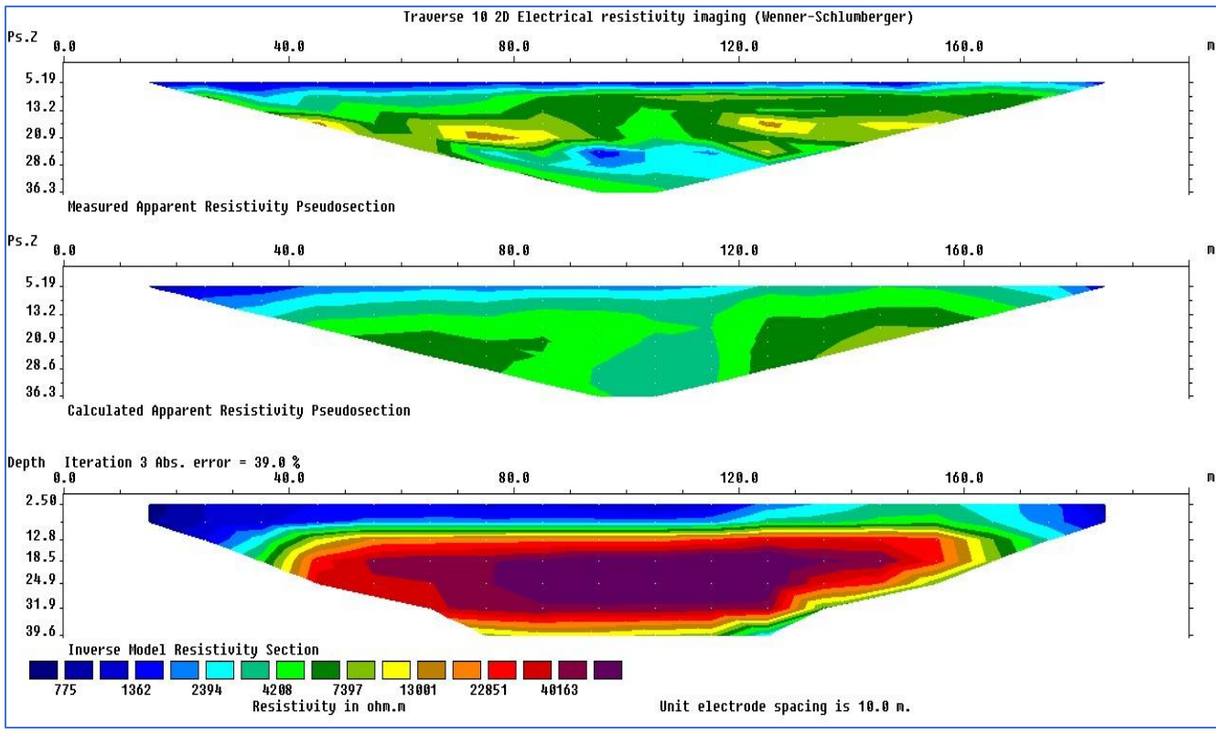

Figure 4.10: 2-D Electrical Resistivity Structure Along Traverse Ten.

Figure 4.10 represents the 2D resistivity image obtained for profile ten with a horizontal distance of 200m and a depth of 39.6m, with a moderate resistivity value to a very high resistivity value across the profile of 775Ωm – 40163Ωm

At the top layer a moderate to high resistivity values ranging from 775 Ωm-4208 Ωm at a depth of 2.50m to 18.5m alluvial, laterite, sandstone and shale was inferred. At a depth of 18.5m to 39.6m a cave like structure suspected to be filled with consolidated sandstone, shale and other rocks having a resistivity value of 22851 Ωm – 40163 Ωm including a minute quantity of clay was inferred.

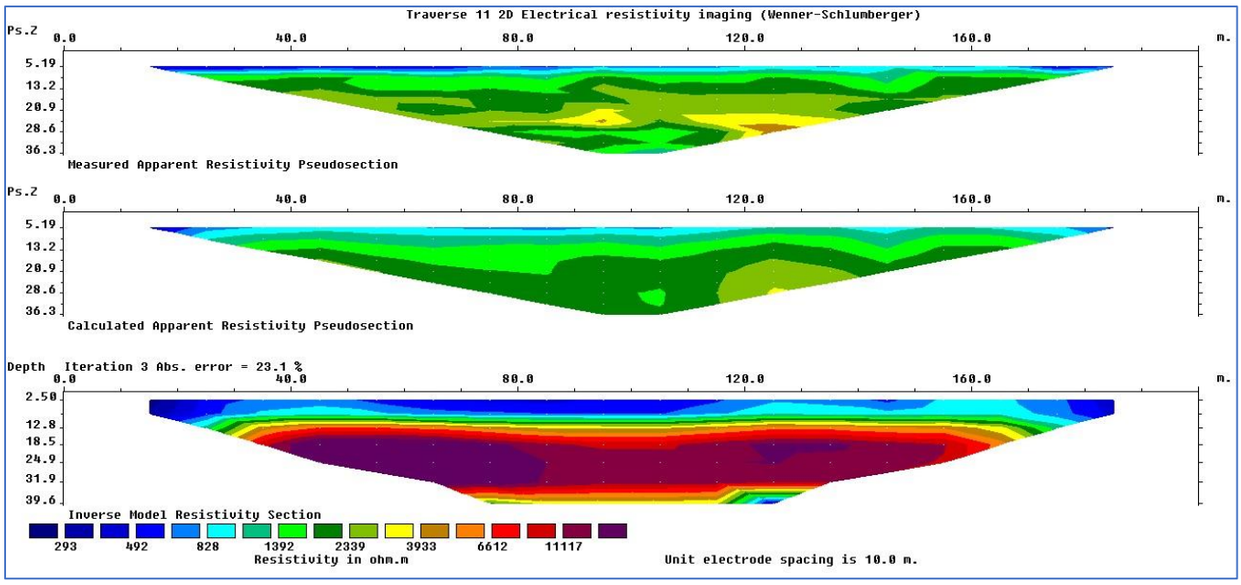

Figure 4.11: 2-D Electrical Resistivity Structure Along Traverse Eleven.

Figure 4.11 represents the 2D resistivity image obtained for profile eleven with a horizontal distance of 200m and a depth of 39.6m, with a moderate resistivity value to a high resistivity value across the profile of 293Ωm – 11117Ωm

At the top layer a moderate to high resistivity values ranging from 293Ωm-3933 Ωm at a depth of 2.50m to 20m alluvial, laterite, sandstone and shale was inferred. At a depth from 20m to 39.6m rocks suspected to have a very high resistivity values were inferred indicating the presence of consolidated sandstone, shale, clayey sand with resistivity values ranging from 3933 Ωm-11117 Ωm.

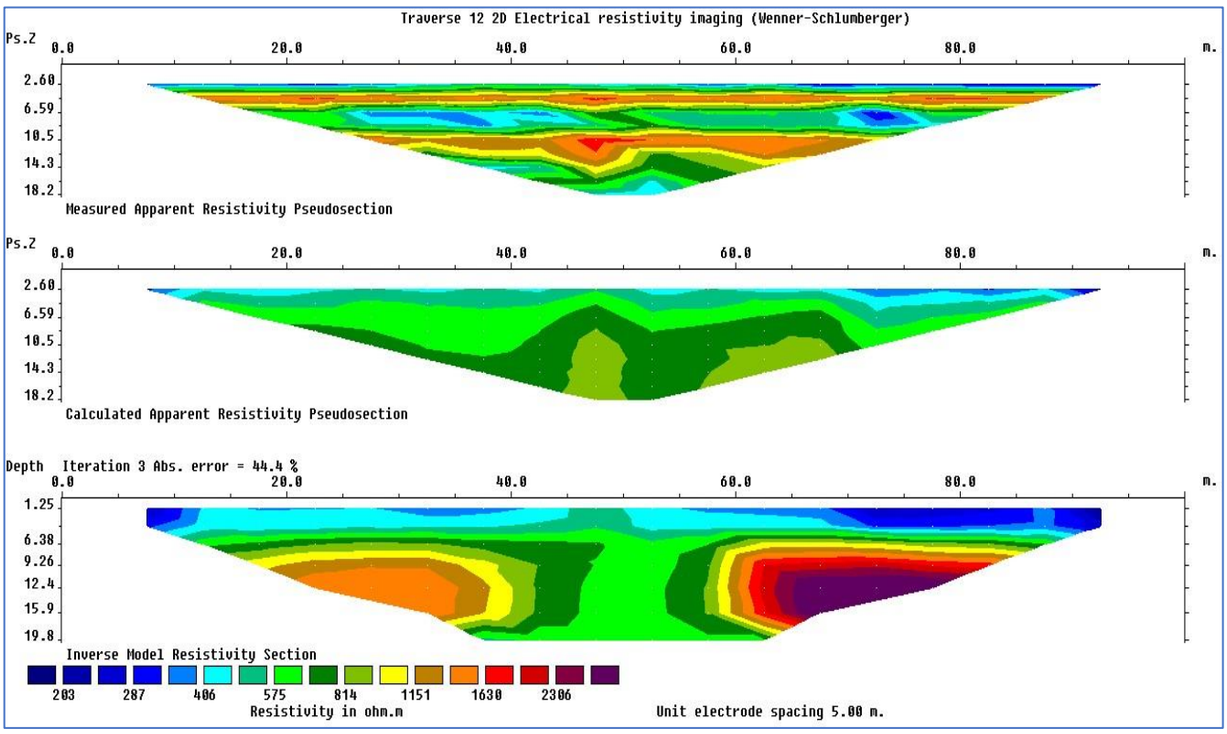

Figure 4.12: 2-D Electrical Resistivity Structure Along Traverse Twelve.

Figure 4.12 represents the 2D resistivity image obtained for profile twelve with a horizontal distance of 100m and a depth of 19.8m, with a moderate to high resistivity values across the profile of 203Ωm – 2306Ωm

At the top layer a moderate to high resistivity values ranging from 203Ωm-814 Ωm at a depth of 1.25m penetrating down to the last depth thereby making alluvial, laterite, to be suspected. At a depth of 9.26m to 15.9m rocks suspected to have a high resistivity value was inferred indicating the presence of unconsolidated sandstone, shale, clayey sand with resistivity values ranging from 1151 Ωm-2306 Ωm.

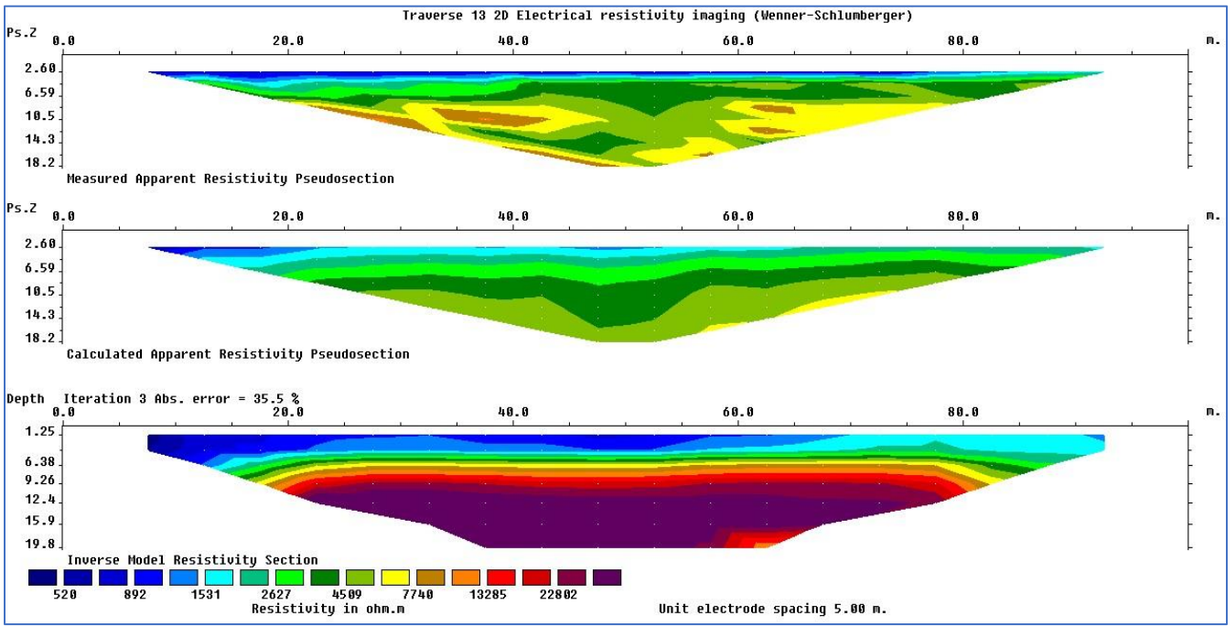

Figure 4.13: 2-D Electrical Resistivity Structure Along Traverse Thirteen.

Figure 4.13 represents the 2D resistivity image obtained for profile thirteen with a horizontal distance of 100m and a depth of 19.8m, with a moderate to a very high resistivity values across the profile of 520Ωm – 22802Ωm

At the top layer a moderate to high resistivity values ranging from 520Ωm-7740 Ωm at a depth of 1.25m to 12.4m thereby making alluvial, laterite, to be suspected. At a depth of 9.26m to 19.8m rocks suspected to have a very high resistivity values was inferred indicating the presence of consolidated sandstone, shale, having a resistivity values of 13285 Ωm-22802 Ωm.

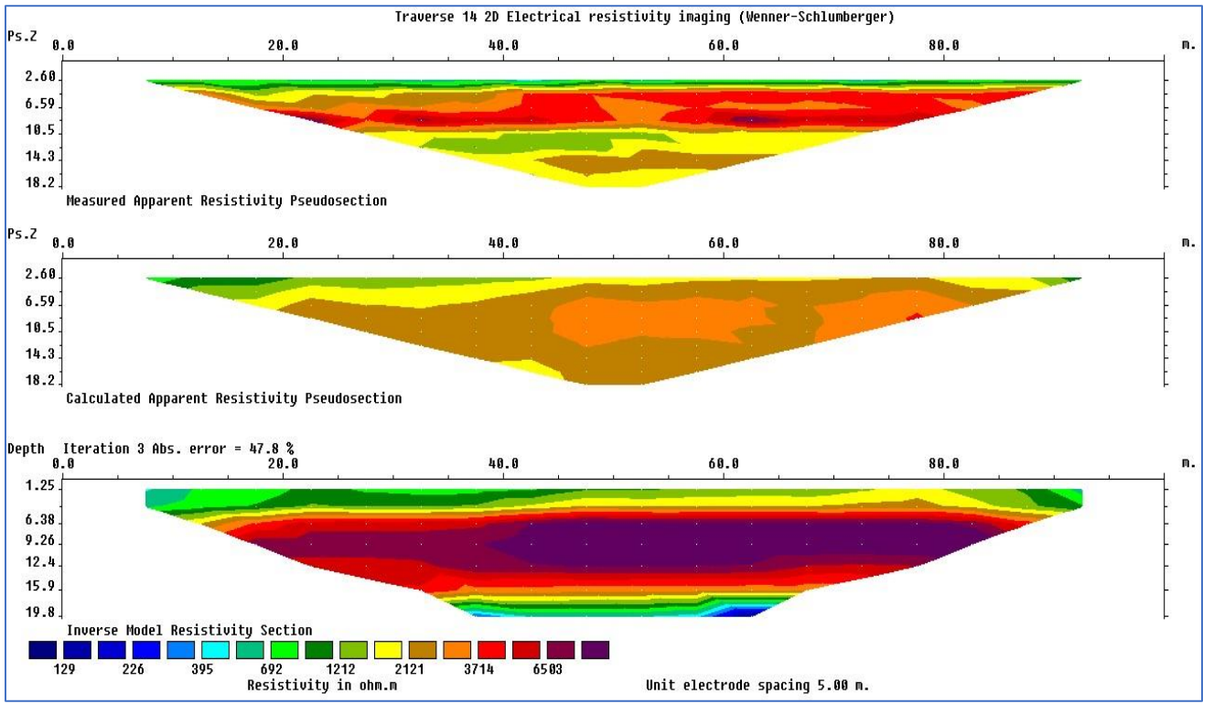

Figure 4.14: 2-D Electrical Resistivity Structure along Traverse Fourteen.

Figure 4.14 represents the 2D resistivity image obtained for profile fourteen with a horizontal distance of 100m and a depth of 19.8m, with moderate to very high resistivity values across the profile of 129Ωm – 6503Ωm

At the top layer, moderate to high resistivity values ranging from 129Ωm-2121 Ωm at a depth of 1.25m to 6.26m thereby making alluvial, laterite, to be suspected. At a depth of 9.26m to 19.8m rocks suspected to have very high resistivity values were inferred indicating the presence of consolidated sandstone, and shale, having resistivity values of 3714 Ωm-6503 Ωm.

4.2 DISCUSSION (REMOTE SENSING)

4.2.1 Digital Elevation Model

The digital elevation model (DEM) provides general information on the topographic nature of the study area. Bojie *et al.*, (1995) proposed that GIS analysis could help organize erosion surveys and mapping by integrating DEM, slope, aspect and land use in the proper GIS platform. The area is characterized as high and low elevation which in turn gives a better view to understanding the digital terrain of the area. Beside it is used to determine the area that is prone to flood during the rainy season (Eteh *et al.*, 2019).

The figures, 4.21 to 4.26 represent the Digital Elevation Model map showing the Normalized Difference Vegetation Index of the study area indicating the areas/sites that are less and more prone to gully erosion. The map comprises five zones red to green. The areas/zones with red color indicate areas that are more prone to gully erosion, the areas with yellow color are moderately prone to gully erosion while areas with green color are less prone to gully erosion. A total of four years NDVI (Normalized Differential Vegetation Index) of different seasons was calculated, fig 4.21 2014 dry season, fig 4.22 2018 dry season, fig 4.23 2019 dry season, fig 4.24 2018 rainy season, fig 4.25 2022 dry season and fig 4.26 2022 rainy season.

Table 4.1: Calculated values of NDVI

YEAR	DRY SEASON	RAINY SEASON
2014	High: 0.458108 Low: 0.0462959	----------
2018	High: 0.340976 Low: 0.0515495	High: 0.6927126 Low: 0.102622
2019	High: 0.704567 Low: 0.132947	----------
2022	High: 0.672547 Low: 0.0176445	High: 0.73443 Low: -0.0596546

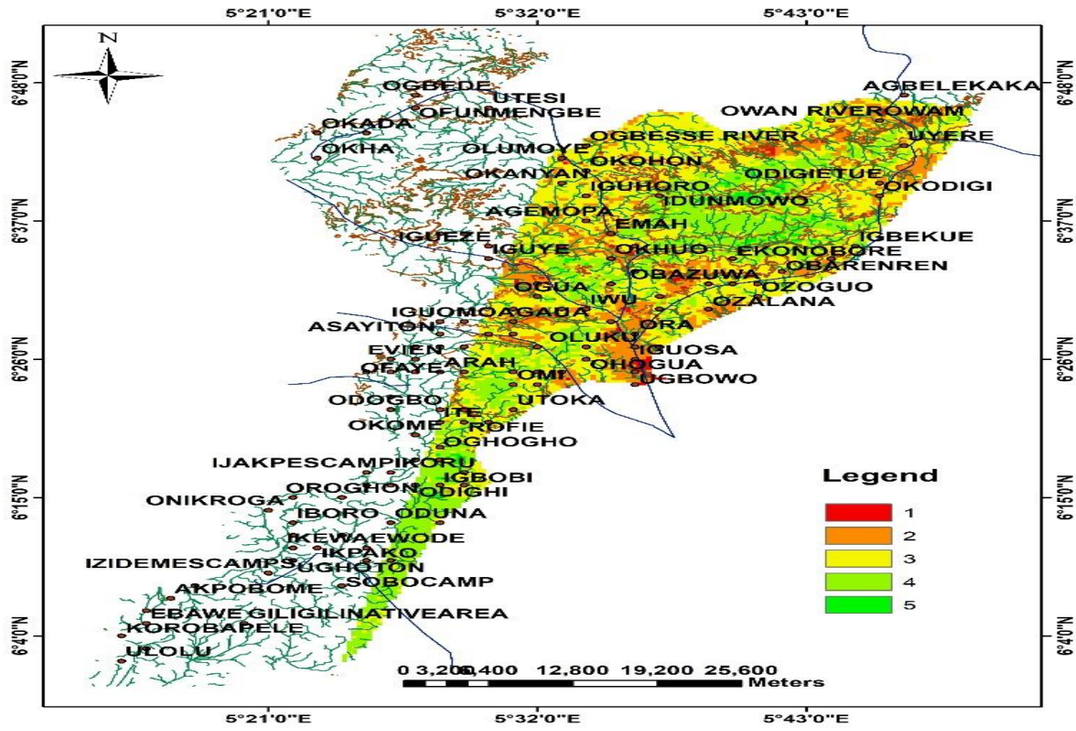

Figure 4.21: Calculated NDVI Dem Map for 2014 dry season.

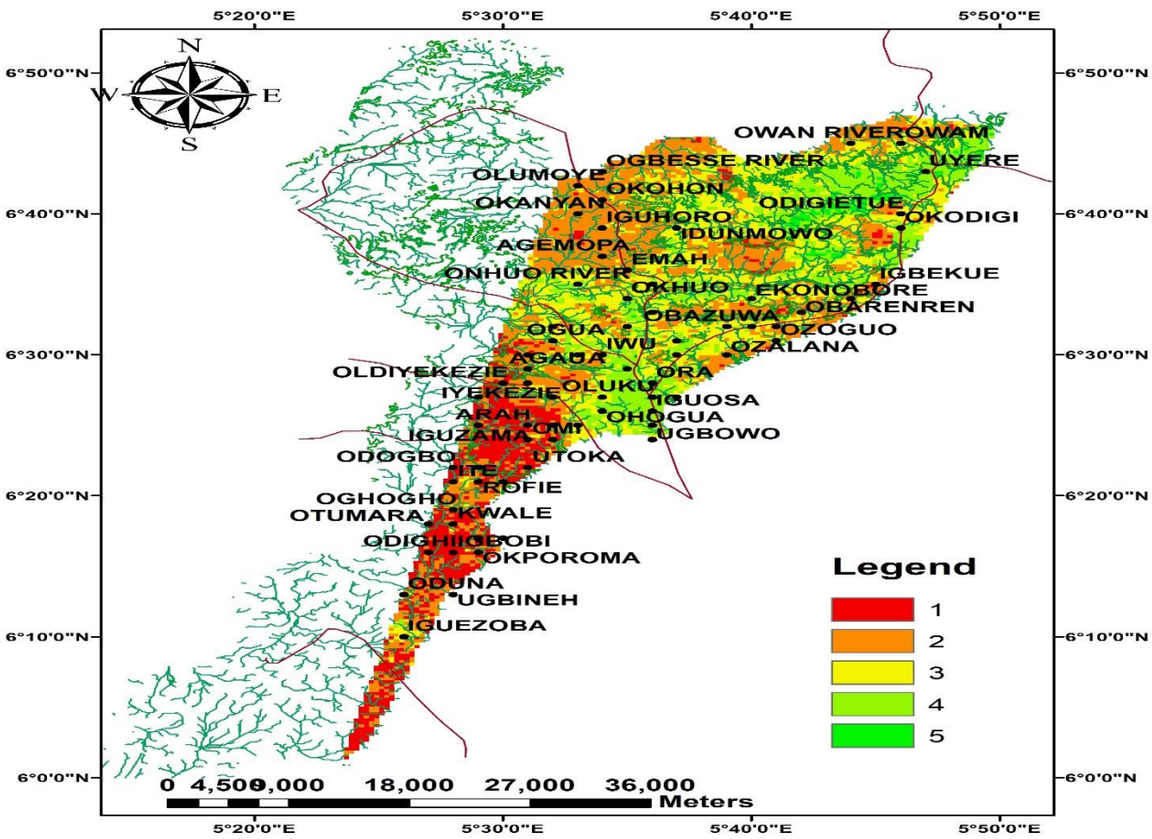

Figure 4.22: Calculated NDVI Dem Map for 2018 dry season.

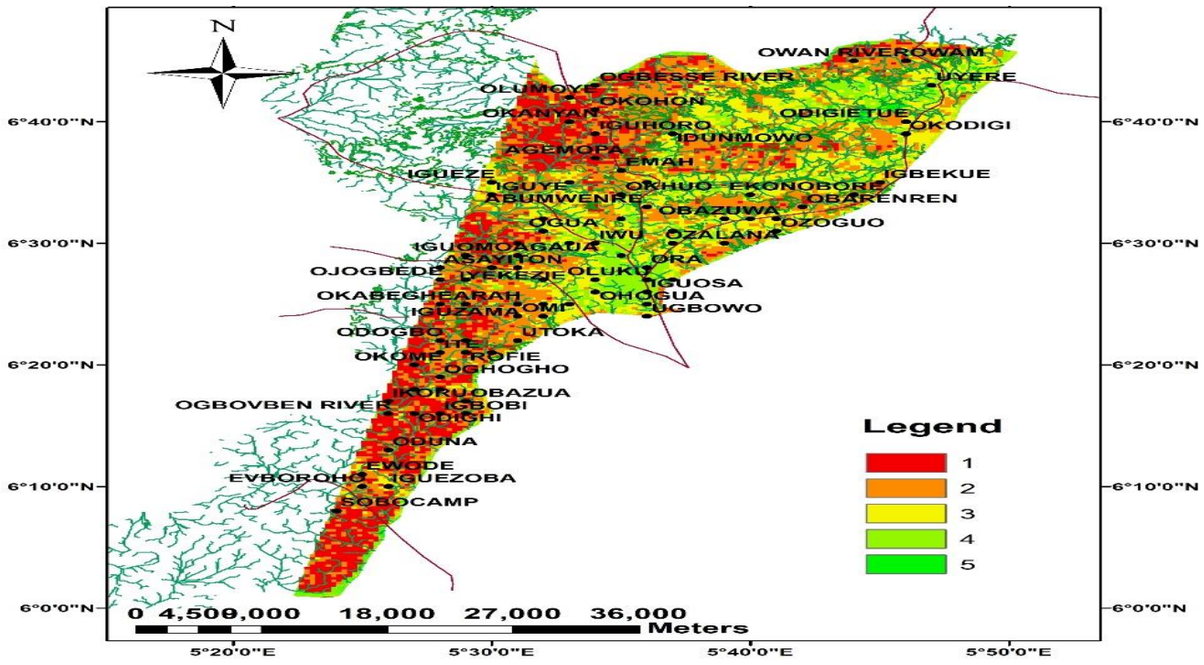

Figure 4.23: Calculated NDVI Dem Map for 2019 dry season.

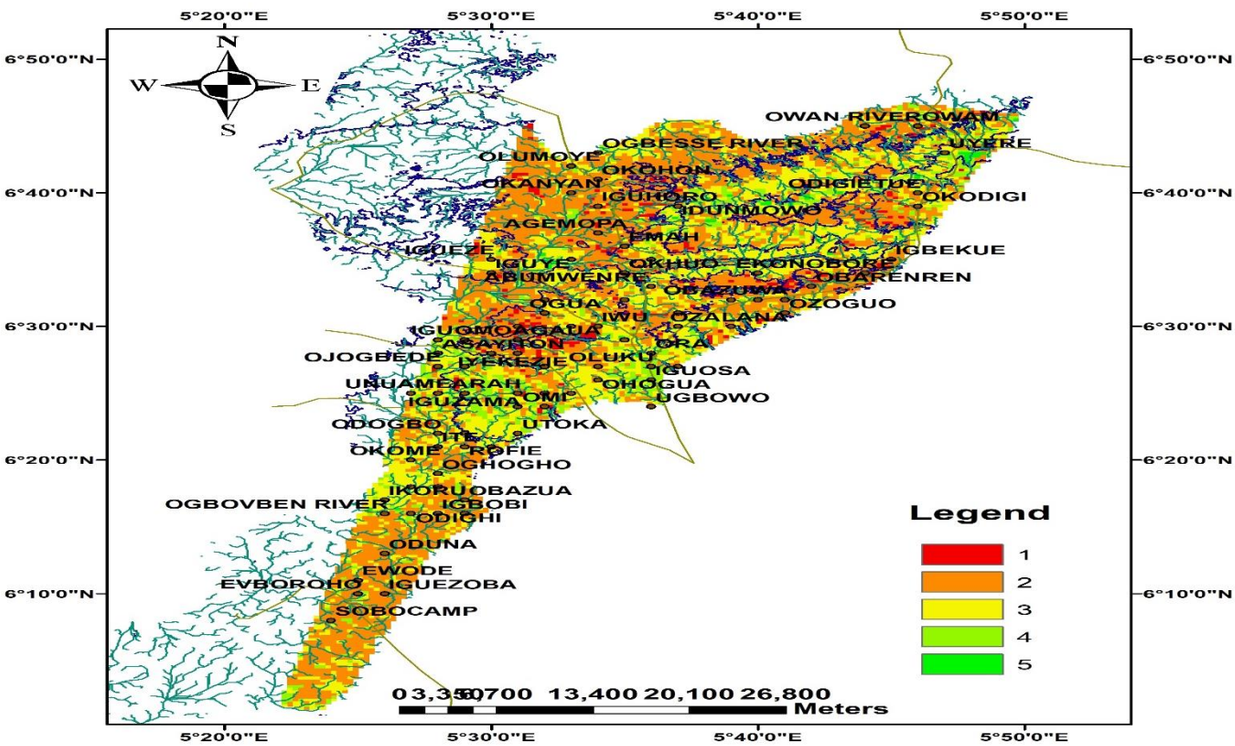

Figure 4.24: Calculated NDVI Dem Map for 2018 rainy season.

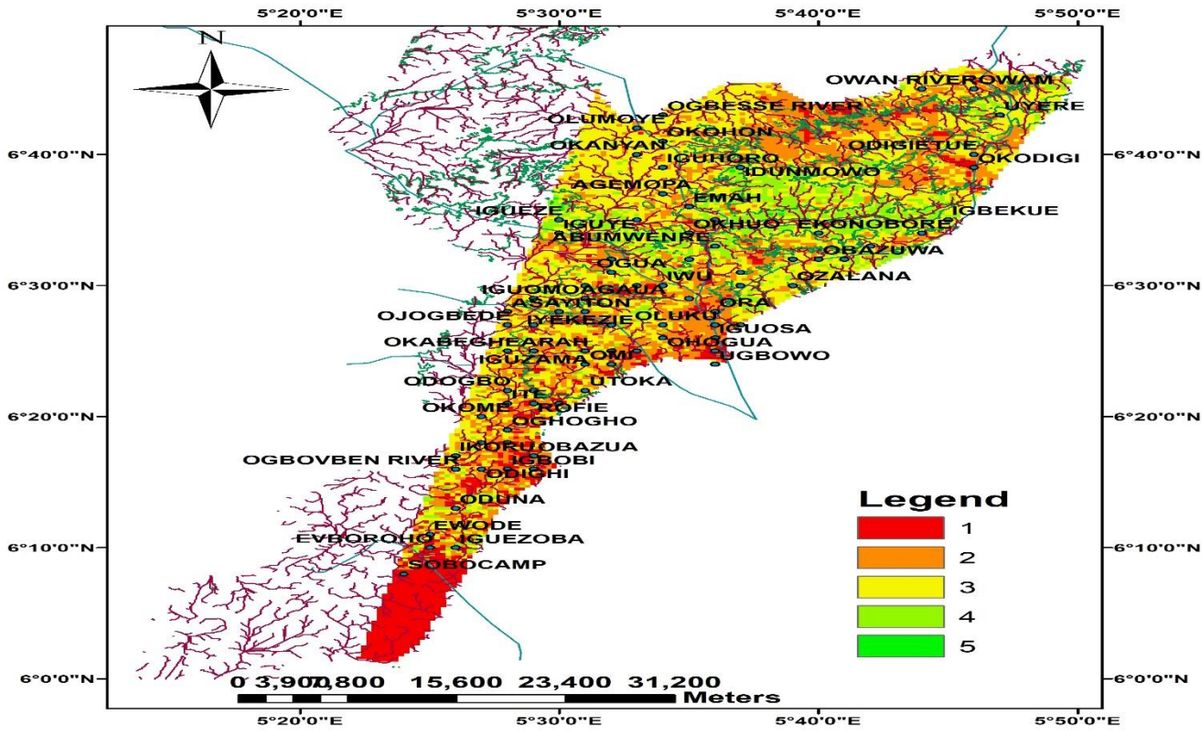

Figure 4.25: Calculated NDVI Dem Map for 2022 dry season.

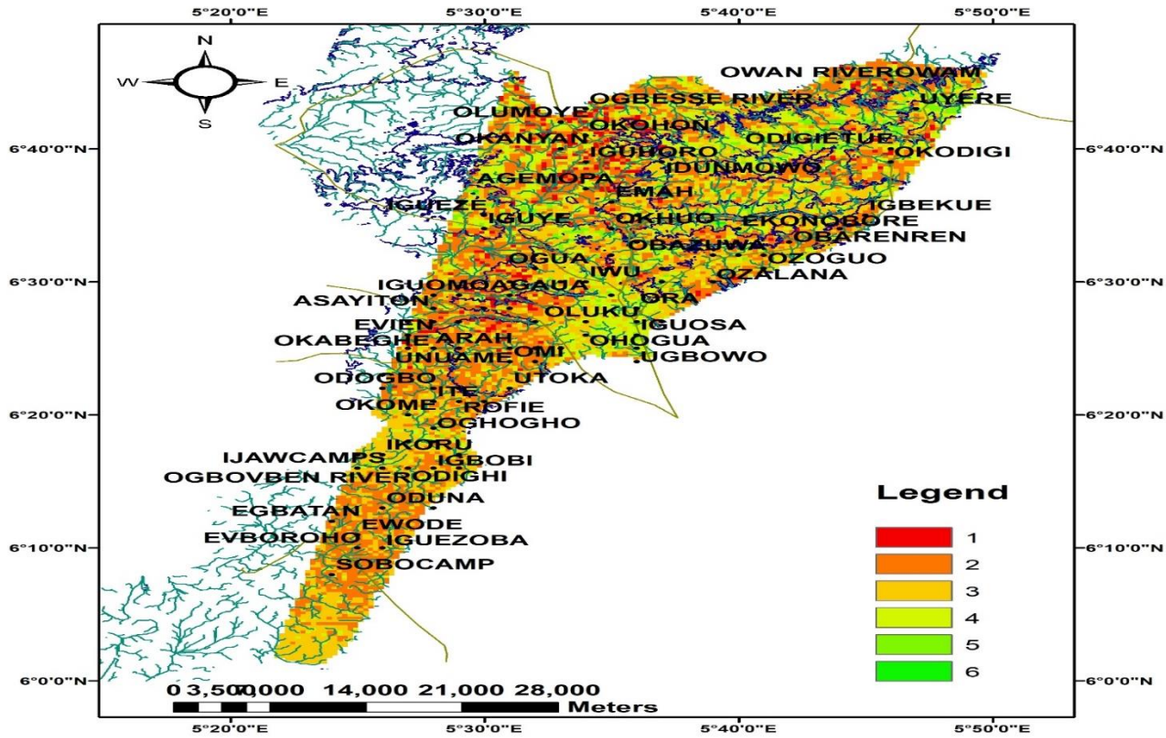

Figure 4.26: Calculated NDVI Dem Map for 2022 rainy season.

CHAPTER FIVE

FINDINGS, CONCLUSION, AND SUGGESTIONS FOR FURTHER STUDIES.

5.1 FINDINGS

In this study the following findings were made:

1. From the inverted 2-D resistivity structure we infer that the first four layers is made up of rocks with low resistivity values indicating the presence of alluvium and laterite and possibly some traceable amount of clay.
2. Comparing the result obtained from 2D resistivity image with the result from remote sensing, it is observed that the low resistivity values as obtained from the 2D indicates the possibility of erodibility potential due to gully.
3. From the 2D resistivity image we infer a traceable amount of clay deposit close to the surface (at a depth of 12.6 – 31.9m) and a quite significant value as we go down the depth (31.9m - 39.6m) indicating that majorly sand (alluvium and Laterite) to be the possibly cause for gully in the area.

5.2 CONCLUSION

Fourteen profiles were occupied for the 2D Electrical Resistivity Imaging (ERI) using Wenner - Schlumberger array which were interpreted using RES2DINV and showing possibly areas prone to gully as observed from low resistivity values.

The DEM map shows that low value of 1 indicates gully prone areas.

The remote sensing techniques gives insight into the development of the gully over a period of time and estimate the extent of gully in the location.

This approach has provided a understanding in the development and gully susceptibility of the study area than would be achieved with a single method of investigation.

The geoelectric sections of the interpreted 2D data from the location delineates the lithostratigraphy of the study area predominantly sand to a depth of about 27m while the

2D resistivity model of all traverses within the gully site reveals low resistive zones with true resistivity values of 100 ohm-m indicative of high erodibility.

5.3 CONTRIBUTION TO KNOWLEDGE

1. It was seen from this research work that the study area is rich in some valuable rocks.
2. The work could be a useful reference point for any structural development that maybe embarked upon at the location in the future.

5.4 SUGGESTIONS FOR FURTHER STUDIES

The following are suggestions for further studies:

1. The same investigation should be carried out periodically to monitor the extent to which the gully erosion develops in relation to flooding.
2. Transient Electromagnetic (EM), and Magnetic Resonance Sounding should be carried out to determine the mineralogy of the clay in the study areas.
3. The government should carry out and fund the effective techniques and measures for the remediation of gullies in the study area before fully reclaiming the gully sites and using it for proper development.

5.5 RECOMMENDATION

1. It is recommended that a larger spread of electrode beyond 200m should be taken in order to get a deeper view of the earth subsurface.
2. Other geophysical resistivity array method should be employed in the study area for comparative characterization of the subsurface.
3. A 3D model of the subsurface should be carried out for relevant information which is able to guide point selection of the best array method to adopt for erosion site investigation.
4. Good drainage system should be constructed to channel off floods into natural basins.

5. Remote sensing and GIS-based multi-criteria analysis should be applied in monitoring areas threatened by gullies incorporating other geophysical methods for fast approach to stiffness of soil.

REFERENCES

Abdulfatai, I. A., Okunlola, I. A., Akande, W. G., Momoh1, L. O., and Ibrahim, K. O. (2014). Review of Gully Erosion in Nigeria: Causes, Impacts and Possible Solutions. Journal of Geosciences and Geomatics Vol2(3): 125-129

Adel O., Dietrich S., Christian S., Volker H. & Michael M. (2022): A GIS-based simulation and visualization tool for the assessment of gully erosion processes. Journal of Spatial Science, DOI: 10.1080/14498596.2022.2133020

Ademilua O. (2018). Geotechnical characterization of subgrade soils in Southwestern Part of Nigeria. Proceedings of frst and second international conferences of the Nigerian Association of Engineering Geology and the Environment, Lagos, Nigeria 1:42–48

Adeniran K.A., Amodu M.F, Adeniji F.A (2010). Water requirements of some selected crops in Kampe dam irrigation project. Australian Journal of Agricultural Engineering. 4(1):119 125

Ahzegbobor, P.I. (2010). 2D and 3D geoelectrical resistivity imaging: Theory and field design. Vol. 5(23), pp. 3592-3606

Aigbadon, G.O., Ocheli, A. and Akudo, E.O (2021). Geotechnical evaluation of gully erosion and landslides materials and their impact in Iguosa and its environs, southern Nigeria. Environ Syst Res 10, 36 (2021). https://doi.org/10.1186/s40068-021-00240-6

Aigbogun, C.O., Alile O.M. and Egbai, J.C. (2017). Geoelectrical Imaging for Shallow Site Investigation at Ekiugbo in Uhunmwode Local Government Area of Edo State, Nigeria. J. Appl. Sci. Environ. Manage. 21 (5): 873-876

Aizebeokhai, P.A., Olayinka A.I., and Singh V.S. (2017). Application of 2D and 3D geolectrical resistivity imaging for engineering site investigation using orthogonal 2D profiles. SEG Expanded Abstracts, 2009, 28, 1440-1444

Akpan O. (2005). Relationship between road pavement failures, engineering indices and underlying geology in a tropical environment. Glob J GeolSci 3(2):99–108

Akpoborie I.A. (2011) Aspects of the Hydrology of the Western Niger Delta Wetlands: Groundwater Conditions in the Neogene (Recent) Deposits of the Ndokwa Area. Proceedings. of the Environmental Management Conference, Federal University of Agriculture, Abeokuta, 13 p.

Alile O.M. and Amadasun, C. V. O. (2007). Direct Current Probing of the Subsurface Earth for Water Bearing Layer in the Oredo Local Government Area, Edo State, Nigeria. Nigerian Journal of Applied Science, 25. pp. 107-116.

Alile O.M., Amadasun, C.V.O. and Evbuomwan, A.L. (2008). Application of Vertical Electrical Sounding Method to Decipher the Existing Subsurface Stratification and Groundwater Occurrence Status in a Location in Edo North of Nigeria. Int. J. Phys. Sci., 3(10): 245–249.

Alile, O. M., Ujuanbi O. and Evbuomwan I. A. (2011). Geoelectric investigation of groundwater in Obaretin – Iyanomon locality, Edo state, Nigeria. Journal of Geology and Mining Research, 3(1), pp. 13 – 20.

Allen J.R.L. (1965) Late Quaternary Niger Delta and Adjacent Areas: Sedimentary Environments and Lithofacies. Bulletin American Association of Petroleum Geology, 49, 547-600. https://doi.org/10.1306/A663363A-16C0-11D7-8645000102C1865D

Amajor L.C. (1991) Aquifers in the Benin Formation (Miocene-Recent) Eastern Niger Delta, Nigeria: Lithostratigraphy, Hydraulics, and Water Quality. Environmental Geology and Water Sciences, 17, 85-101. https://doi.org/10.1007/BF01701565

Arulbalaji P., Padmalal D. and Sreelash K. (2019) GIS and AHP Techniques Based Delineation of Groundwater Potential Zones: A Case Study from Southern Western Ghats, India. Scientific Reports, 9, 2082. https://doi.org/10.1038/s41598-019-38567-x

Avbovbo, A.A. & Ayoola, O. (1981), "Petroleum prospects of the southern Nigeria's Anambra Basin", Oil Gas Journal (79) 334–347.

Awosike, L.F. (1995) Impact of Global Climate Change and Sea Level Rise on Coastal Resources and Energy Development in Nigeria.

Ayolabi E.A. (2013). Engineering site Characterization using 2D and 3D Electrical Resistivity Tomography. Earth Science Research Vol 2n1. pp.133

Bojie F., Xilin W. and Gulinck H. (1995): Soil erosion types in the loess hill and gully area of China. J Environ Sci 7:266–272

Boniface, C. E., Akudo E. O., and Hycienth O. N. (2019). Gully Erosion and Landslides in Southeastern Nigeria: Causes, Consequences and Control Measures.

Bryant E. A (1991). Natural Hazards. Cambridge: Cambridge University Press, 167–170

Burrough, P.A. (1986) Principles of Geographical Information Systems for Land Resources Assessment. Oxford University Press, Oxford.

Chorley R. J. and Barry R. G. (1987): Atmosphere, Weather and Climate, 5^{e} éd., Methuen, New York, 460 p., ill., 4 app., 15,5 x 23 cm. ISBN 0-416-97142-2

Chude, V.O., Ezendu C.O., Ugadu, M.E and Adiaha, M.S. (2021). A Review of the menace of soil erosion in Nigeria with specific reference to Southeastern States. Nigeria Institute of Soil Science Colloquia SSSN 44, 405-414

Crozier M.J (1986). Landslides: causes, consequences & environment. Taylor & Francis.

Dahlin T. and Loke M.H. (1998). Resolution of 2D Wenner resistivity imaging as assessed by numerical modelling, Journal of Applied Geophysics, 38, 237-249.

Egwuonwu, G.N., Okoyeh, E.I. and Chikwelu E. E. (2019). 2DNear-Surface Litho-Structural Geophysical Investigation at the Vicinities of Two Gully-Erosion/Landslide Sites in South Eastern Nigeria. IOSR Journal of Applied Geology and Geophysics (IOSR-JAGG) 7.5 (2019): 70-75

Eleraki1, M., Gadallah, M.M., Gemail, K.S., and Attwa, M. (2010). Application of resistivity method in environmental study of the appearance of soil water in the central part of Tenth of Ramadan City, Egypt. Quarterly Journal of Engineering Geology and Hydrogeology 43(2):171-184.

Eteh, D., Francis, E.E. and Francis O. (2019). Determination of flood hazard Zones Using Geographical Information Systems and Remote Sensing techniques: A case Study in part of Yenagoa Metropolis, 21(1): 1-9.

Ferhat O. and Tazegul O. (2011). Geophysical analysis of the soils for civil (Geotechnical) engineering and urban planning purposes: Some case histories from Turkey. International Journal of the Physical Sciences Vol. 6(5), pp. 1169-1195, DOI: 10.5897/IJPS11.090

Griffiths D.H. and Barker R.D. (1993). Two-dimensional resistivity imaging and modeling in areas of complex geology. Journal of Applied Geophysics, 29:211–226

Heywood I. (1998) Introduction to geographic Information Systems, 4th edition pg 22.

Igbokwe, J.I., Ojiako J.C., Nnodu V.C (2003). Monitoring, Characterization and Controlling of Floodwater Erosion Using Remote Sensing Techniques. Proceedings of the Technical Session of the 38th Annual General Meeting and Conference of Nigerian Institution of Surveyors, Lokoja pp. 123-134.

Johnbosco C. Egbueri & Ogbonnaya Igwe (2021). The impact of hydrogeomorphological characteristics on gullying processes in erosion-prone geological units in parts of southeast Nigeria, Geology, Ecology, and Landscapes, 5:3, 227-240, DOI: 10.1080/24749508.2020.1711637

Kearey P. and Brooks M. (1991). An introduction to geophysical exploration, 2nd Editions, Blackwell Scientific Publications, Oxford, 254-263pp.

Krhoda, G. (2013). Landslides in densely populated county at the foot slopes of Mount Elgon (Uganda): Characteristics and causal factors. Journal of Geomorphology 73:149–165.

Lillesand T.M. and Kiefer, R.W. (1994) Remote Sensing and Image Interpretation. 3rd Edition, John Wiley and Sons, Inc., Hoboken, 750.

Lillesand T.M. and Kiefer, R.W. (2000) Remote Sensing and Image Interpretation. John Wiley & Sons, New York.

Linus U. (2020). Erosion crisis swallowed homes and livelihoods in Nigeria, Climate Home News, Viewed 20 Aug. 2022, https://www.climatechangenews.com/2020/01/20/erosion crisis-swallows-homes-livelihoods-Nigeria/

Loke M.H. and Dahlin T. (2002) A comparison of the Gauss-Newton and Quasi-Newton Methods in Resistivity Imaging Inversion, Journal of Applied Geophysics, 49, 149–162.

Loke, M.H (2003). Application of Electrical Resistivity Tomography in engineering, archaeological, environmental and geological problems. Exploration Geophysics 34(1):182-187

Maina, M. B (2022). Surveillance of Gully Erosion in Damagum Town and Environs, Fune Local Government Area, Yobe State of Nigeria. Dutse Journal of Pure and Applied (DUJOPAS), Vol. 8(2b): 116-130

Marescot L., Monnet R. and Chapellier D. (2008). Resistivity and induced polarization surveys for slope instability studies in the Swiss Alps. Engineering Geology - ENG GEOL. 98. 18-28. 10.1016/j.enggeo.2008.01.010.

Mbaya, L.A. (2013). A Study of Inter-relations among Gully Variables in Gombe town, Gombe State, Nigeria. Wudpecker J Geogr. Regional Plan. 1(1):001-006.

Meshida E.A (2006). Highway failure over talc–tremolite schist terrain: a case study of the Ife to Ilesha Highway, Southwestern Nigeria. Bull EngGeol Environ 65:457–461. https://doi. org/10.1007/s10064-005-0037-7

Modak, P., Mandal M., Mandi S. and Ghosh B. (2022). Gully erosion vulnerability modelling, estimation of soil loss and assessment of gully morphology: a study from cratonic part of eastern India. Environmental Science Pollution Research International. doi: 10.1007/s11356-022-22118-5.

Msilimba G. (2002). Landslides geohazard assessment of the Vunguvungu/Banga catchment area in Rumphi District, MSc. Environmental Science Thesis. University of Malawi, Zomba.

Msilimba, G.G. and Holmes, P.J (2005). A landslide hazard assessment and vulnerability appraisal procedure: Vunguvungu/Banga catchment, Northern Malawi. Natural hazards, 34(2), pp.199-216.

Nosipho, P.M (2018). Remote Sensing of Gully Erosion in the Communal Lands of Okhombe Valley, Drakensberg, South Africa. University of KwaZulu – Natal.

NTA News, Sunday July 6, 2013.

Nwankwoala, H. O., Ahiakwo E., Akudo E. O., Okeke, C. and Abija, F. A (2022). Geological and geotechnical assessment of gully erosion sites in parts of Uturu, Southeastern Nigeria. African Journal of Engineering Research Vol. 10(2), pp. 17-23.

Ofomata, G.E.K. (1981). Acrtual and Potential erosion in Nigeria and measures for control. Soil Science Society of Nigeria Special Monograph 1, 151-165.

Okagbue C.O (1992). The 1988 Nanka landslide, Anambra State, Nigeria. Bulletin of the International Association of Engineering Geology 46(1): 79-87

Omon E.J and Ogheruemusua G.J (2014). Evaluating soil erosion in the Benin metropolis, Edo State. Int J Phys Sci 2(3):38–45

Omosuyi G.O., Adeyemo A. and Adegoke A.O. (2007). Investigation of ground water prospect using electromagnetic and geoelectric sounding at Afunbiowo. PacJSci Technol.8:172–182.

Ozsoy, G., Aksoy, E., Dirim, M.S. and Tumsavas, Z. (2012). Determination of soil erosion risk in the Mustafakemalpasa River Basin, Turkey, using the revised universal soil loss equation, geographic information system, and remote sensing. Environmental Management, 50(4):679-94. doi: 10.1007/s00267-012-9904-8

Panda K.P, Sharma S, Jha M.K (2018). Mapping of laterite zones using 2D electrical resistivity tomography survey in parts of Paschim Medinipur, West Bengal, Indian: An approach for artificial groundwater recharge. J Earth Syst Sci 129,119

Perrone A., Lapenna V. L. and Sarah P. (2014). Electrical resistivity tomography technique for landslide investigation: A review. Earth-Science Reviews. 135. 10.1016/j.earscirev.2014.04.002.

Poesen J. (2011). Challenges in gully erosion research. Journal of Landform Analysis 17(5-9)

Reijers T.J.A. (2011) Stratigraphy and Sedimentology of the Niger Delta. Geologos, 17, 133-162. https://doi.org/10.2478/v10118-011-0008-3

Reyment, R.A. (1965). Aspects of the Geology of Nigeria, Ibadan University Press.

Seutloali, K. E., Dube T. and Mutanga O. (2017). Assessing and mapping the severity of soil erosion using the 30-m Landsat multispectral satellite data in the former South African homelands of Transkei. Physics and Chemistry of the Earth, Parts A/B/C, 100, 296-304.

Shi Z. H., Fang N. F., Wu F. Z., Wang L., Yue B. J., and Wu G. L. (2012). Soil erosion processes and sediment sorting associated with transport mechanisms on steep slopes. Journal of Hydrology, 454, 123-130.

Uwaezuoke, C.C., K.S. Ishola and E. A. Ayolabi (2021). Electrical resistivity imaging and multichannel analysis of surface waves for mapping the subsurface of a Wetland Area of Lagos, Nigeria, NRIAG. Journal of Astronomy and Geophysics, 10:1, 300 319, DOI: 10.1080/20909977.2021.1927427

Wenfu P., Jieming Z., Zhengwei H., and Cun-jian Y. (2008). Integrated Use of Remote Sensing and GIS for Predicting Soil Erosion Process. The International Archives of the Photogrammetry, Remote Sensing and Spatial Information Sciences. Vol. XXXVII. Part B4. Beijing.

Whiteman A. (1982) Nigeria: Its Petroleum Geology, Resources and Potential. I and II. Graham and Trotman Ltd., London. http://dx.doi.org/10.1007/978-94-009-7361-9.

APPENDIX

TRAVERSE 1 LONG. 005°37'42.63" LAT. 06°24'06.56' 'Elev. 73m					
Electrode Location a = 10, n = 1, k = 62.84					
C1	P1	P2	C2	R (Ω)	ρ (Ωm)
0	10	20	30	4.3	270.212
10	20	30	40	8.7	546.708
20	30	40	50	6.5	408.46
30	40	50	60	11	691.24
40	50	60	70	8.2	515.288
50	60	70	80	10.5	659.82
60	70	80	90	7	439.88
70	80	90	100	7.8	490.152
80	90	100	110	11.2	703.808
90	100	110	120	16.5	1036.86
100	110	120	130	19.5	1225.38
110	120	130	140	23.5	1476.74
120	130	140	150	22.6	1420.18
130	140	150	160	25.4	1596.14
140	150	160	170	19.8	1244.23
150	160	170	180	22.8	1432.75
160	170	180	190	18.8	1181.39
170	180	190	200	19	1193.96
Electrode Location a = 10, n = 2, k = 188.52					
C1	P1	P2	C2	R (Ω)	ρ (Ωm)
0	20	30	50	1.8	339.336
10	30	40	60	1.4	263.928
20	40	50	70	1.4	263.928
30	50	60	80	1.5	282.78

40	60	70	90	1.7	320.484
50	70	80	100	1.6	301.632
60	80	90	110	1.4	263.928
70	90	100	120	2.5	471.3
80	100	110	130	5.3	999.156
90	110	120	140	4.3	810.636
100	120	130	150	3.5	659.82
110	130	140	160	5.9	1112.27
120	140	150	170	7.9	1489.31
130	150	160	180	5.2	980.304
140	160	170	190	5.3	999.156
150	170	180	200	4.3	810.636
Electrode Location a = 10, n = 3, k = 377.04					
C1	P1	P2	C2	R (Ω)	ρ (Ωm)
0	30	40	70	0.405	152.701
10	40	50	80	0.53	199.831
20	50	60	90	0.409	154.209
30	60	70	100	0.492	185.504
40	70	80	110	0.464	174.947
50	80	90	120	0.96	361.958
60	90	100	130	1.4	527.856
70	100	110	140	2.3	867.192
80	110	120	150	1.5	565.56
90	120	130	160	1.4	527.856
100	130	140	170	2.3	867.192
110	140	150	180	3.8	1432.75
120	150	160	190	2.1	791.784

130	160	170	200	2.2	829.488
Electrode Location a = 10, n = 4, k = 628.4					
C1	P1	P2	C2	R (Ω)	ρ (Ωm)
0	40	50	90	0.25	157.1
10	50	60	100	0.867	544.823
20	60	70	110	0.265	166.526
30	70	80	120	2.46	1545.86
40	80	90	130	0.328	206.115
50	90	100	140	1.3	816.92
60	100	110	150	0.731	459.36
70	110	120	160	0.548	344.363
80	120	130	170	0.645	405.318
90	130	140	180	0.764	480.098
100	140	150	190	1.7	1068.28
110	150	160	200	0.964	605.778
Electrode Location a = 10, n = 5, k = 942.6					
C1	P1	P2	C2	R (Ω)	ρ (Ωm)
0	50	60	110	0.23	216.798
10	60	70	120	0.164	154.586
20	70	80	130	0.222	209.257
30	80	90	140	0.187	176.266
40	90	100	150	0.864	814.406
50	100	110	160	0.316	297.862
60	110	120	170	0.212	199.831
70	120	130	180	0.442	416.629
80	130	140	190	0.424	399.662
90	140	150	200	0.593	558.962
Electrode Location a = 10, n = 6, k = 1319.64					

C1	P1	P2	C2	R (Ω)	ρ (Ωm)
0	60	70	130	0.192	253.371
10	70	80	140	0.143	188.709
20	80	90	150	0.151	199.266
30	90	100	160	0.442	583.281
40	100	110	170	0.776	1024.04
50	110	120	180	0.698	921.109
60	120	130	190	0.309	407.769
70	130	140	200	0.311	410.408
Electrode Location a = 10, n = 7, k = 1759.52					
C1	P1	P2	C2	R (Ω)	ρ (Ωm)
0	70	80	150	0.142	249.852
10	80	90	160	0.051	89.7355
20	90	100	170	0.185	325.511
30	100	110	180	0.197	346.625
40	110	120	190	0.164	288.561
50	120	130	200	0.069	121.407
Electrode Location a = 10, n = 8, k = 2262.24					
C1	P1	P2	C2	R (Ω)	ρ (Ωm)
0	80	90	170	0.156	352.909
10	90	100	180	0.194	438.875
20	100	110	190	0.045	101.801
30	110	120	200	0.18	407.203
Electrode Location a = 10, n = 9, k = 2827.8					
C1	P1	P2	C2	R (Ω)	ρ (Ωm)
0	90	100	190	0.094	265.813
10	100	110	200	0.086	243.191
TRAVERSE 1 LONG. 005˚37'47.79'' LAT. 06˚24'05.18'' Elev. 64m					

TRAVERSE 2 LONG. 005˚37'38.43" LAT. 06˚24'06.26" Elev. 96m					
Electrode Location a = 10, n = 1, k = 62.84					
C1	P1	P2	C2	R (Ω)	ρ (Ωm)
0	10	20	30	8.25	518.43
10	20	30	40	8.75	549.85
20	30	40	50	12.9	810.636
30	40	50	60	12.4	779.216
40	50	60	70	12.65	794.926
50	60	70	80	12.4	779.216
60	70	80	90	11.45	719.518
70	80	90	100	11.85	744.654
80	90	100	110	11	691.24
90	100	110	120	12.25	769.79
100	110	120	130	11.25	706.95
110	120	130	140	13.1	823.204
120	130	140	150	12.45	782.358
130	140	150	160	13.35	838.914
140	150	160	170	13.65	857.766
150	160	170	180	12.25	769.79
160	170	180	190	11.85	744.654
170	180	190	200	11.15	700.666
Electrode Location a = 10, n = 2, k = 188.52					
C1	P1	P2	C2	R (Ω)	ρ (Ωm)
0	20	30	50	6.25	1178.25
10	30	40	60	7.2	1357.34
20	40	50	70	6.8	1281.94
30	50	60	80	6.15	1159.4

40	60	70	90	7.2	1357.34
50	70	80	100	5.45	1027.43
60	80	90	110	8.3	1564.72
70	90	100	120	7.45	1404.47
80	100	110	130	6.95	1310.21
90	110	120	140	3.05	574.986
100	120	130	150	3.1	584.412
110	130	140	160	7.5	1413.9
120	140	150	170	9.5	1790.94
130	150	160	180	9	1696.68
140	160	170	190	6.65	1253.66
150	170	180	200	5.5	1036.86
Electrode Location a = 10, n = 3, k = 377.04					
C1	P1	P2	C2	R (Ω)	ρ (Ωm)
0	30	40	70	0.805	303.517
10	40	50	80	0.503	189.651
20	50	60	90	0.609	229.617
30	60	70	100	0.592	223.208
40	70	80	110	0.465	175.324
50	80	90	120	0.956	360.45
60	90	100	130	1.7	640.968
70	100	110	140	2.1	791.784
80	110	120	150	1.9	716.376
90	120	130	160	1.8	678.672
100	130	140	170	2.8	1055.71
110	140	150	180	3.2	1206.53
120	150	160	190	2.6	980.304

130	160	170	200	1.9	716.376
Electrode Location a = 10, n = 4, k = 628.4					
C1	P1	P2	C2	R (Ω)	ρ (Ωm)
0	40	50	90	0.342	214.913
10	50	60	100	0.768	482.611
20	60	70	110	0.356	223.71
30	70	80	120	0.286	179.722
40	80	90	130	0.556	349.39
50	90	100	140	1.8	1131.12
60	100	110	150	0.655	411.602
70	110	120	160	0.468	294.091
80	120	130	170	0.556	349.39
90	130	140	180	0.757	475.699
100	140	150	190	1.5	942.6
110	150	160	200	1.1	691.24
Electrode Location a = 10, n = 5, k = 942.6					
C1	P1	P2	C2	R (Ω)	ρ (Ωm)
0	50	60	110	0.334	314.828
10	60	70	120	0.243	229.052
20	70	80	130	0.286	269.584
30	80	90	140	0.211	198.889
40	90	100	150	1.1	1036.86
50	100	110	160	0.432	407.203
60	110	120	170	0.332	312.943
70	120	130	180	0.521	491.095
80	130	140	190	0.388	365.729
90	140	150	200	0.633	596.666
Electrode Location a = 10, n = 6, k = 1319.64					

C1	P1	P2	C2	R (Ω)	ρ (Ωm)
0	60	70	130	0.187	246.773
10	70	80	140	0.221	291.64
20	80	90	150	0.168	221.7
30	90	100	160	0.554	731.081
40	100	110	170	0.833	1099.26
50	110	120	180	0.688	907.912
60	120	130	190	0.423	558.208
70	130	140	200	0.286	377.417
Electrode Location a = 10, n = 7, k = 1759.52					
C1	P1	P2	C2	R (Ω)	ρ (Ωm)
0	70	80	150	0.198	348.385
10	80	90	160	0.122	214.661
20	90	100	170	0.212	373.018
30	100	110	180	0.202	355.423
40	110	120	190	0.188	330.79
50	120	130	200	0.108	190.028
Electrode Location a = 10, n = 8, k = 2262.24					
C1	P1	P2	C2	R (Ω)	ρ (Ωm)
0	80	90	170	0.165	373.27
10	90	100	180	0.222	502.217
20	100	110	190	0.098	221.7
30	110	120	200	0.099	223.962
Electrode Location a = 10, n = 9, k = 2827.8					
C1	P1	P2	C2	R (Ω)	ρ (Ωm)
0	90	100	190	0.079	223.396
10	100	110	200	0.094	265.813
TRAVERSE 2 LONG. 005˚37'44.34" LAT. 06˚24'05.23" Elev. 95m					

TRAVERSE 3 LONG. 005˚37'47.17" LAT. 06˚24'01.56" Elev. 96m					
Electrode Location a = 10, n = 1, k = 62.84					
C1	P1	P2	C2	R (Ω)	ρ (Ωm)
0	10	20	30	10.65	669.246
10	20	30	40	13	816.92
20	30	40	50	13.2	829.488
30	40	50	60	13.55	851.482
40	50	60	70	16.7	1049.43
50	60	70	80	13.7	860.908
60	70	80	90	16.7	1049.43
70	80	90	100	15.55	977.162
80	90	100	110	16.7	1049.43
90	100	110	120	16.7	1049.43
100	110	120	130	34.7	2180.55
110	120	130	140	27.9	1753.24
120	130	140	150	17.6	1105.98
130	140	150	160	15.2	955.168
140	150	160	170	12.75	801.21
150	160	170	180	12.85	807.494
160	170	180	190	11.25	706.95
170	180	190	200	14	879.76
Electrode Location a = 10, n = 2, k = 188.52					
C1	P1	P2	C2	R (Ω)	ρ (Ωm)
0	20	30	50	15.55	2931.49
10	30	40	60	16.7	3148.28
20	40	50	70	16.7	3148.28
30	50	60	80	34.7	6541.64

40	60	70	90	27.9	5259.71
50	70	80	100	17.6	3317.95
60	80	90	110	15.2	2865.5
70	90	100	120	12.75	2403.63
80	100	110	130	12.85	2422.48
90	110	120	140	11.25	2120.85
100	120	130	150	14	2639.28
110	130	140	160	12.6	2375.35
120	140	150	170	14.45	2724.11
130	150	160	180	15.4	2903.21
140	160	170	190	13.25	2497.89
150	170	180	200	13.1	2469.61
Electrode Location a = 10, n = 3, k = 377.04					
C1	P1	P2	C2	R (Ω)	ρ (Ωm)
0	30	40	70	1.8	678.672
10	40	50	80	6.3	2375.35
20	50	60	90	4.5	1696.68
30	60	70	100	2.3	867.192
40	70	80	110	2.5	942.6
50	80	90	120	2.9	1093.42
60	90	100	130	2.6	980.304
70	100	110	140	2.8	1055.71
80	110	120	150	2.7	1018.01
90	120	130	160	2.5	942.6
100	130	140	170	2.2	829.488
110	140	150	180	1.8	678.672
120	150	160	190	2.8	1055.71

130	160	170	200	2.6	980.304
Electrode Location a = 10, n = 4, k = 628.4					
C1	P1	P2	C2	R (Ω)	ρ (Ωm)
0	40	50	90	0.895	562.418
10	50	60	100	0.885	556.134
20	60	70	110	0.875	549.85
30	70	80	120	0.805	505.862
40	80	90	130	0.825	518.43
50	90	100	140	0.801	503.348
60	100	110	150	0.875	549.85
70	110	120	160	0.832	522.829
80	120	130	170	0.743	466.901
90	130	140	180	0.722	453.705
100	140	150	190	0.655	411.602
110	150	160	200	0.532	334.309
Electrode Location a = 10, n = 5, k = 942.6					
C1	P1	P2	C2	R (Ω)	ρ (Ωm)
0	50	60	110	0.565	532.569
10	60	70	120	0.695	655.107
20	70	80	130	0.735	692.811
30	80	90	140	0.695	655.107
40	90	100	150	0.745	702.237
50	100	110	160	0.735	692.811
60	110	120	170	0.732	689.983
70	120	130	180	0.691	651.337
80	130	140	190	0.684	644.738
90	140	150	200	0.734	691.868
Electrode Location a = 10, n = 6, k = 1319.64					

C1	P1	P2	C2	R (Ω)	ρ (Ωm)
0	60	70	130	0.686	905.273
10	70	80	140	0.763	1006.89
20	80	90	150	0.704	929.027
30	90	100	160	0.655	864.364
40	100	110	170	0.515	679.615
50	110	120	180	0.386	509.381
60	120	130	190	0.511	674.336
70	130	140	200	0.286	377.417
Electrode Location a = 10, n = 7, k = 1759.52					
C1	P1	P2	C2	R (Ω)	ρ (Ωm)
0	70	80	150	0.225	395.892
10	80	90	160	0.254	446.918
20	90	100	170	0.265	466.273
30	100	110	180	0.248	436.361
40	110	120	190	0.262	460.994
50	120	130	200	0.276	485.628
Electrode Location a = 10, n = 8, k = 2262.24					
C1	P1	P2	C2	R (Ω)	ρ (Ωm)
0	80	90	170	0.176	398.154
10	90	100	180	0.108	244.322
20	100	110	190	0.177	400.416
30	110	120	200	0.189	427.563
Electrode Location a = 10, n = 9, k = 2827.8					
C1	P1	P2	C2	R (Ω)	ρ (Ωm)
0	90	100	190	0.144	407.203
10	100	110	200	0.139	393.064
TRAVERSE 3 LONG. 005°37'49.21" LAT. 06°24'07.38" Elev. 91m					